

Diffractive photoproduction of J/ψ and Υ using holographic QCD: gravitational form factors and GPD of gluons in the proton

Kiminad A. Mamo* and Ismail Zahed†

Department of Physics and Astronomy, Stony Brook University, Stony Brook, New York 11794-3800, USA

(Dated: October 11, 2019)

We present a holographic analysis of diffractive photoproduction of charmonium J/ψ and upsilononium Υ on a proton, considered as a bulk Dirac fermion, for all ranges of \sqrt{s} , i.e., from near threshold to very high energy. Using the bulk wave functions of the proton and vector mesons, within holographic QCD, and employing Witten diagrams in the bulk, we compute the diffractive photoproduction amplitude of J/ψ and Υ . The holographic amplitude shows elements of the strictures of vector meson dominance (VMD). It is dominated by the exchange of a massive graviton or 2^{++} glueball resonances near threshold, and its higher spin- j counterparts that reggeize at higher energies. Both the differential and total cross sections are controlled by the gravitational form factor $A(t)$, and compare well to the recent results reported by the GlueX collaboration near threshold and the world data at large \sqrt{s} . The holographic gravitational form factors, including the D-term, which is due to the exchange of massive spin-0 glueballs, are in good agreement with lattice simulations. We use it to extract the holographic pressure and shear forces inside the proton. Finally, using a pertinent integral representation of the holographic gravitational form factor $A(t)$ near threshold, and its Pomeron counterpart way above threshold, we extract the generalized parton distribution (GPD) of gluons inside the proton at different resolutions.

PACS numbers:

I. INTRODUCTION

Exclusive production of heavy mesons such as charmonia and bottomonia through the use of photo- or electroproduction processes provides the optimal framework for diffractive physics. In the limit when the coherence length of the virtual photon is large in comparison to the proton size, the scattering virtual photon on a hadron is equivalent to the scattering of a hadron onto a hadron. The process is mostly dominated by the exchange of gluons with vacuum quantum numbers, leading to a slowly rising cross section at high energy. The rise is due to the exchange of a Pomeron, an effective object lying on the highest Regge trajectory. First principle perturbative QCD calculations [1, 2] provide insights to the nature of this exchange, although the softness of the exchange suggests an altogether non-perturbative approach.

Soft electroproduction on a nucleon is analogous to a hadron of varying size scattering off a nucleon, with a virtual photon wavefunction of squared transverse size $1/Q^2$. In the photoproduction limit with $Q^2 \rightarrow 0$, the size is hadronic and non-perturbative physics applies. The diffractive and non-perturbative production process whereby the soft virtual photon turns to a heavy meson is analogous to the scattering of two dipoles with light-cone wavefunctions for the in-out virtual photon states. It is inherently non-perturbative at small Q^2 . Throughout, we will focus on electroproduction close to the photon point or photoproduction for heavy mesons such as char-

monium and bottomium.

Holographic QCD provides a non-perturbative framework for discussing structure and scattering of hadrons. It stems from a conjecture that observables in strongly coupled gauge theories in the limit of a large number of colors, can be determined from classical fields interacting through gravity in generally an anti-de-Sitter space in higher dimensions [3]. The original conjecture was put forth and demonstrated for conformal $\mathcal{N} = 4$ Yang-Mills theory, and argued by many to hold under some assumptions for non-conformal gauge theories such as QCD. Exclusive production of heavy mesons has been analyzed in the context of holographic QCD at high energy [4, 5], where the exchange reggeizes [6–13]. Diffractive production of vector mesons in the non-holographic context can be found in [14].

Recently, the GlueX collaboration has put forth measurements of threshold charmonium production using virtual photons close to the photon point [15]. Additional measurements at JLab in this channel with higher accuracy using the SoLID detector should improve further the statistics [16]. One purpose of these experiments is the extraction of the gluonic component entering the composition of the nucleon mass. In this spirit, a new analysis of these threshold data was carried in [17, 18] using a hybrid holographic construction combining general QCD arguments and lattice results. One of the purposes of this paper is to carry an analysis of the new GlueX data near threshold [15] and the existing world data well above threshold, all within a holographic QCD model using the bottom-up approach. This analysis complements the earlier investigations in [4, 5] at high energy, all the way to threshold. For completeness, we note the earlier suggestion to use the photoproduction process near threshold

*Electronic address: kiminad.mamo@stonybrook.edu

†Electronic address: ismail.zahed@stonybrook.edu

to probe the gluon content of the nucleon [19].

The holographic photoproduction amplitude is dominated by the exchange of a massive 2^{++} graviton at threshold, and higher spin- j exchanges away from threshold that rapidly reggeize. The 0^{++} glueballs are found to decouple owing to their vanishing coupling to the virtual photons, while the dilatons are shown to decouple from the bulk Dirac fermion. At threshold, the holographic photoproduction amplitude directly probes a pertinent gravitational form factor which maps on the gluonic contribution to the energy momentum tensor of the nucleon as a Dirac fermion in the bulk.

This paper consists of several new results: 1/ The derivation of all three holographic gravitational form factors and their comparison to recent lattice data; 2/ The derivation of the gluonic pressure and shear forces inside the proton; 3/ The derivation that the holographic processes $\gamma p \rightarrow Vp$ and $\gamma p \rightarrow \gamma^* p$ are related in bulk by vector meson dominance (VMD); 4/ The derivation of the holographic photoproduction differential and total cross sections for J/Ψ and their comparison to current data for all energies; 5/ The derivation that the threshold cross section is dominated by only one invariant gravitational form factor $A(t)$, due to the exchange of a 2^{++} glueball in bulk; 6/ The extraction of the value of $A(0)$ from the data for different brane embeddings; 7/ The derivation of the holographic gluonic GPD of the nucleon as a bulk Dirac fermion; 8/ The prediction for the diffractive photoproduction of Υ .

The organization of the paper is as follows: In section II we review the kinematics for a general $2 \rightarrow 2$ process. In section III, we detail the general structures of the Witten diagrams for exclusive process, like the diffractive photoproduction of J/ψ , by using the bulk wave functions of hadrons in holographic QCD. In section IV, we introduce in detail the bottom holographic model we use, and derive the bulk vertices for the Witten diagrams from the bulk action of the model. In section V, we derive the holographic gravitational form factors using Witten diagrams, and compare them to the recent lattice results. In section VI, we use our holographic D-term to calculate the pressure distribution and shear forces inside the proton. In section VII, we show how vector meson dominance (VMD) holds in the present holographic construction, and derive the scattering amplitude for the diffractive photoproduction by approximating the bulk-to-bulk glueball propagator near the boundary which will enable us to write down the scattering amplitude explicitly in terms of the gravitational form factor $A(t)$ of spin-2 glueball exchanges. In section VIII, the photoproduction differential and total cross sections close to the photon point are detailed at threshold in the single graviton exchange limit. In section IX, we generalize the result beyond threshold through reggeization by including the higher spin- j exchanges and their re-summation. In section X, we derive the gluonic GPD from a pertinent integral representation of the form factor $A(t)$. Our conclusions are in section XI, and details

of the calculations are given in several appendices.

II. KINEMATICS OF THE $\gamma^* p \rightarrow Vp$ PROCESS

Throughout, we will refer to real and virtual photoproduction by γ^* in the general presentation, but we will specialize to photoproduction in most of the specific analyses and results. All our arguments extend readily to diffractive electroproduction of heavy mesons $V = J/\Psi, \Upsilon$ with minor changes.

We start by briefly reviewing the kinematics for the process $\gamma^* p \rightarrow Vp$. We first define the Lorentz scalars as $s = W^2 = (p_1 + q_1)^2$, and $t = (p_1 - p_2)^2 = (q_1 - q_2)^2$ where $q_{1,2}$ are the four-vectors of the virtual photon and vector meson, respectively (note that we occasionally use the notation $q \equiv q_1$ and $q' \equiv q_2$), and $p_{1,2}$ are the four vector of the proton. Throughout we will work with mostly negative signature, i.e., $\eta_{\mu\nu} = (+1, -1, -1, -1)$. Note that our convention is different from the mostly positive signature used in most holographic analyses.

We will work in the center-of-mass (CM) frame of the pair composed of the virtual photon γ^* and the proton. In this frame, one can derive the mathematical relationships between the three-momenta of the virtual photon and vector meson ($\mathbf{q}_\gamma, \mathbf{q}_V$) and Lorentz scalars ($s, t, q_1^2 = -Q^2, q_2^2 = M_V^2, p_1^2 = p_2^2 = m_N^2$) as (see, for example, Eqs.11.2-4 in [20])

$$|\mathbf{q}_\gamma| = \frac{1}{2\sqrt{s}} \sqrt{s^2 - 2(-Q^2 + m_N^2)s + (-Q^2 - m_N^2)^2}, \quad (\text{II.1})$$

$$|\mathbf{q}_V| = \frac{1}{2\sqrt{s}} \sqrt{s^2 - 2(M_V^2 + m_N^2)s + (M_V^2 - m_N^2)^2}, \quad (\text{II.2})$$

and

$$t = -Q^2 + M_V^2 - 2E_\gamma E_V + 2|\mathbf{q}_\gamma||\mathbf{q}_V| \cos \theta, \quad (\text{II.3})$$

Here $E_\gamma = (-Q^2 + \mathbf{q}_\gamma^2)^{\frac{1}{2}}$ is the energy of the virtual photon, and $E_V = (M_V^2 + \mathbf{q}_V^2)^{\frac{1}{2}}$ is the energy of the vector meson. The t -transfer at low \sqrt{s} is bounded by $t_{\min} \equiv |t|_{\cos \theta = +1}$ and $t_{\max} \equiv |t|_{\cos \theta = -1}$ as illustrated in Fig. 1.

We now note that at threshold and for example $V = J/\Psi$ with $s_{\text{tr}} = (m_N + M_V)^2 = 4.04 \text{ GeV}^2$

$$\begin{aligned} -t_{\min}(s = s_{\text{tr}}) &= \frac{m_N M_V^2}{m_N + M_V} \\ &= 1.5^2 \text{ GeV}^2 \ll 4.04^2 \text{ GeV}^2 = s_{\text{tr}} \end{aligned} \quad (\text{II.4})$$

and away from threshold

$$-t_{\min}(s \gg s_{\text{tr}}) \sim \left(\frac{m_N M_V}{s} \right)^2 \ll s \quad (\text{II.5})$$

The photoproduction kinematics for charmonium and also bottomium, is dominated by the diffractive process all the way to threshold.

The differential cross section for the photoproduction process $\gamma^* p \rightarrow V p$ is given by (see for example, Eq.11.34 in [20])

$$\frac{d\sigma}{dt} = \frac{e^2}{64\pi s |\mathbf{q}_\gamma|^2} |\mathcal{A}_{\gamma^* p \rightarrow V p}(s, t)|^2. \quad (\text{II.6})$$

and the total cross section for small \sqrt{s} close to threshold is

$$\sigma(s) = \int_{t_{\min}}^{t_{\max}} dt \left(\frac{d\sigma}{dt} \right). \quad (\text{II.7})$$

We now show how to use Witten diagrams in AdS with bulk wavefunctions for the vector mesons, bulk-to-boundary and bulk-to-bulk propagators within pertinent holographic models in the bottom-up approach.

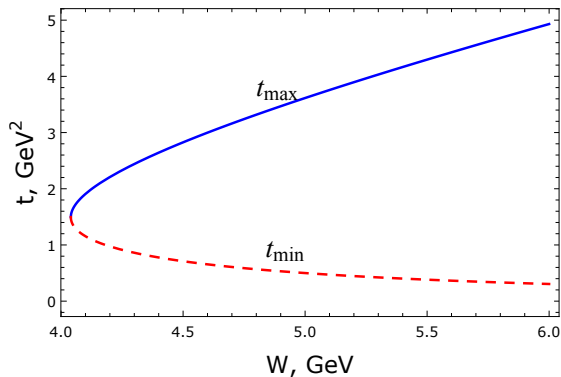


FIG. 1: t_{\min} and t_{\max} vs $W = \sqrt{s}$ for $M_V = M_{J/\psi} = 3.10 \text{ GeV}$, $m_N = 0.94 \text{ GeV}$, and $Q = 0$. Note that at the threshold energy $W_{\text{tr}} = \sqrt{s_{\text{tr}}} = m_N + M_V = 4.04 \text{ GeV}$, we have $t_{\min} = t_{\max}$.

III. HOLOGRAPHIC PHOTOPRODUCTION OF VECTOR MESONS

The diffractive amplitude for the photoproduction of a vector meson, in a given holographic model of QCD, can be computed by using the Witten diagram shown in Fig. 2, where bulk VMD is manifest as we will detail below. The structure of the Witten diagram is pretty general, and can be applied to any holographic model to QCD with a mass-gap, and a discrete mass spectrum of hadrons.

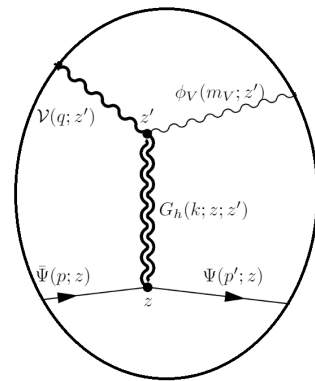


FIG. 2: Witten diagram for the diffractive photoproduction of vector mesons with a bulk wave function ϕ_V . The thick lines or thick wiggles represent the propagators of summed over vector meson or glueball resonances. The thin lines or thin wiggles correspond to a single vector meson and proton. For scalar glueball resonances, due to the dilaton and the trace-full part of the metric fluctuation, we simply replace the bulk-to-bulk propagator $G_h(k, z, z')$ of spin-2 glueballs by $G_{\varphi, f}(k, z, z')$.

The main elements of the Witten diagrams shown in Fig. 2 (also in Figs. 2, 3 for the gravitational form factor) are composed of:

1/ the bulk-to-boundary propagator of the vector mesons (or virtual photons for space-like momenta $q^2 = -Q^2$) as

$$V(q, z) = \mathcal{V}(q = iQ, z) = C_V \times g_5 \sum_n \frac{F_n \phi_n(z)}{Q^2 + m_n^2}, \quad (\text{III.8})$$

where $\phi_n(m_n, z)$, m_n , $f_n \equiv -F_n/m_n$, and g_5 are the bulk wave function, mass, decay constant, and hadronic coupling constant of each meson resonances, respectively. C_V is a normalization constant for the mesons which can be identified with the value of the electromagnetic form factor of the proton at zero-momentum transfer (and $C_V = F_1^{(P)}(Q = 0) = 1$ since the electric charge of the proton is normalized to one in units of e);

2/ the bulk-to-boundary propagator of the spin-2 glueballs (for space-like momenta $k^2 = -K^2$)

$$h(k, z) = \mathcal{H}(K, z) = C_h \times \sqrt{2\kappa} \sum_n \frac{F_n \psi_n(z)}{K^2 + m_n^2}, \quad (\text{III.9})$$

where $\psi_n(m_n, z)$, m_n , $f_n \equiv -F_n/m_n$, and κ are the bulk wave function, mass, decay constant, and hadronic coupling constant of each glueball resonances. C_h is the normalization constant for glueballs (which will be identified with the gravitational form factor of the proton at zero momentum transfer, i.e., $C_h \equiv A(t = 0)$);

3/ the bulk-to-bulk propagators of the vector meson and glueball resonances

$$G_V(q', z, z') = C_V \times \sum_n \frac{\phi_n(z)\phi_n(z')}{q'^2 - m_n^2}, \quad (\text{III.10})$$

and

$$G_h(k, z, z') = C_h \times \sum_n \frac{\psi_n(z)\psi_n(z')}{k^2 - m_n^2}; \quad (\text{III.11})$$

and the bulk wave function of the proton (a Dirac fermion in the bulk) is denoted as $\Psi(p, z)$.

More specifically, for the hard-wall and soft-wall holographic models of QCD, that we focus on in this paper, all the ingredients of the Witten diagram Fig. 2 are determined in terms of their bulk wave functions, the normalization constants $C_{V,h}$, the mass scale parameters z_0 for the hard-wall ($\tilde{\kappa}_{V,N}$ and c_V for the soft-wall), and the hadronic coupling constants g_5 (for mesons) and κ (for glueballs).

The mass scale parameters z_0 or $\tilde{\kappa}_{\rho,N}$ are simultaneously fixed to the proton's and the ρ meson's mass, $\tilde{\kappa}_V$ and c_V for $V = (J/\psi, \Upsilon)$ are fixed by their mass $m_V = (m_{J/\psi}, m_\Upsilon)$ and decay constants $f_V = (f_{J/\psi}, f_\Upsilon)$. The hadronic coupling constant of glueballs κ is fixed by using Type II supergravity action on $AdS_5 \times S^5$, and the hadronic coupling of vector mesons is fixed by using the DBI action for D7 or D9 flavor branes. Finally, we will extract the gravitational form factor $A(0) = C_h/g_5^2$ by comparing the holographic scattering amplitude to experimental data in the low energy regime.

Note that, in general, the normalized bulk wave function of one of the vector meson resonances $\phi_{n=0} \equiv \phi_V$ takes the form

$$\phi_V = c_V z J(M_V z) = \frac{f_V}{M_V} \times M_V z J(M_V z) \quad (\text{III.12})$$

where $J(M_V z)$ is a special function that depends on the details of the holographic model. And, the decay constant f_V , for a meson at rest, defined as

$$\langle 0 | J_{V,i} | V_j \rangle = f_V M_V \delta_{ij} \quad (\text{III.13})$$

is calculable in a given holographic model to QCD, and can be extracted experimentally from the leptonic width as

$$\Gamma(V \rightarrow \ell^+ \ell^-) = \frac{4\pi}{3} \alpha_{QED}^2 e_V^2 \frac{f_V^2}{M_V} \quad (\text{III.14})$$

where e_V is the electric charge of the constituent quarks of the vector meson. For $V = (J/\psi, \Upsilon)$: $e_V = (2/3, 1/3)$, $M_V = (3.097, 9.460)$ GeV and $e_V f_V = (270, 238)$ MeV.

IV. HOLOGRAPHIC MODEL

We consider AdS_5 with a background metric $g_{MN} = (\eta_{\mu\nu}, -1)/z^2$ and $\eta_{\mu\nu} = (1, -1, -1, -1)$. Confinement will be described by a background dilaton $\phi = \tilde{\kappa}_V^2 z^2$ for mesons, $\phi = \tilde{\kappa}_N^2 z^2$ for protons and $\phi = 2\tilde{\kappa}_N^2 z^2$ for glueballs in the soft wall model. In the hard wall model, $\phi = 0$ and confinement is set at $z = z_0$. The bulk graviton and dilaton fields will be described by φ and $h_{\mu\nu}$ respectively, while the bulk U(1) vector gauge field and a spin- $\frac{1}{2}$ Dirac fermion by V^M and Ψ respectively.

A. Bulk Dirac fermion and vector meson

The bulk Dirac fermion action in curved AdS_5 with minimal coupling to the U(1) vector meson is [21]

$$S = \int d^5x \sqrt{g} (\mathcal{L}_F + \mathcal{L}_V) + \int d^4x \sqrt{-g^{(4)}} \mathcal{L}_{UV}, \quad (\text{IV.15})$$

with the fermionic, gauge field and boundary actions

$$\begin{aligned} \mathcal{L}_F &= \frac{1}{2g_5^2} e^{-\phi(z)} \\ &\times \left(\frac{i}{2} \bar{\Psi} e_A^N \Gamma^A (\vec{D}_N - \overleftarrow{D}_N) \Psi - (M + V(z)) \bar{\Psi} \Psi \right), \\ \mathcal{L}_V &= -\frac{1}{4g_5^2} e^{-\phi(z)} g^{\mu\alpha} g^{\beta\nu} F_{\mu\nu}^V F_{\alpha\beta}^V, \\ \mathcal{L}_{UV} &= \frac{1}{2g_5^2} (\bar{\Psi}_L \Psi_R + \bar{\Psi}_R \Psi_L)_{z=\epsilon}, \end{aligned} \quad (\text{IV.16})$$

We have fixed the potential $V(z) = \tilde{\kappa}_N^2 z^2$ for both the hard and soft wall model. We have denoted by $e_A^N = z \delta_A^N$ the inverse vielbein, and defined the covariant derivatives

$$\begin{aligned} \vec{D}_N &= \vec{\partial}_N + \frac{1}{8} \omega_{NAB} [\Gamma^A, \Gamma^B] - iV_N \\ \overleftarrow{D}_N &= \overleftarrow{\partial}_N + \frac{1}{8} \omega_{NAB} [\Gamma^A, \Gamma^B] + iV_N \end{aligned} \quad (\text{IV.17})$$

The components of the spin connection are $\omega_{\mu z\nu} = -\omega_{\mu\nu z} = \frac{1}{z} \eta_{\mu\nu}$, the Dirac gamma matrices satisfy anti-commutation relation $\{\Gamma^A, \Gamma^B\} = 2\eta^{AB}$, that is, $\Gamma^A = (\gamma^\mu, -i\gamma^5)$, and $F_{MN}^V = \partial_M V_N - \partial_N V_M$. The equation of motions for the bulk Dirac fermion and the U(1) gauge field follow by variation

$$\begin{aligned} [ie_A^N \Gamma^A D_N - \frac{i}{2} (\partial_N \phi) e_A^N \Gamma^A - (M + \phi(z))] \Psi &= 0, \\ \frac{1}{\sqrt{g}} \partial_M (\sqrt{g} e^{-\phi} F^{MN}) &= 0. \end{aligned} \quad (\text{IV.18})$$

The coupling g_5 is inherited from the nature of the brane embeddings in bulk: $1/g_5^2 \equiv 3N_c N_f / (12\pi^2)$ (D7-branes), and $1/g_5^2 \equiv (3\sqrt{\lambda}/2^{5/2}\pi)N_c N_f / (12\pi^2)$ (D9-branes). The brane embeddings with $N_f = 1$ are more appropriate for describing heavy mesons in bulk, as the U(1) field mode decompose in an infinite tower of massive vector mesons on these branes as we discussed above. When ignoring these embedding, the standard assignment is: $1/g_5^2 \equiv N_c / (12\pi^2)$.

We note that in (IV.16), we have excluded a Yukawa-type coupling between the dilaton and the bulk Dirac fermion, since neither the fermionic part of the Type IIB supergravity action (see, for example, Eq. A.20 in [22]) nor the fermionic part of the DBI action in string theory (see, for example, Eq. 56 in [23]) support such a coupling.

B. Spectra

The spectrum for the hard wall model is fixed by the zeros of the Bessel function $J_1(m_n z_0) = 0$ and does not Reggeize. It does in the soft wall model by solving the equation of motion for V^N following from (IV.15). The results for the heavy meson masses and decay constants are [24]

$$\begin{aligned} m_n^2 &= 4\tilde{\kappa}_V^2 (n^* + 1) \\ g_5 f_n &= \sqrt{2}\tilde{\kappa}_V \left(\frac{n+1}{n^*+1} \right)^{\frac{1}{2}} \end{aligned} \quad (\text{IV.19})$$

with $n^* = n + c_V^2 / 4\tilde{\kappa}_V^2$. The additional constant c_V is fixed as $c_V^2 / 4\tilde{\kappa}_V^2 = M_V^2 / 4\tilde{\kappa}_V^2 - 1$ for $n = 0$ for the heavy mesons $V = (J/\psi, \Upsilon)$, and $c_V = 0$ for the light mesons. The mass spectrum of the bulk Dirac fermions is given by [21]

$$m_n^2 = 4\tilde{\kappa}_N^2 (n + \tau - 1), \quad (\text{IV.20})$$

with the twist factor τ . For the specific soft wall applications to follow we will set $\tilde{\kappa}_N = \tilde{\kappa}_V = \tilde{\kappa}_\rho$ for simplicity, unless specified otherwise.

C. Bulk graviton and dilaton

The graviton in bulk is dual to a glueball on the boundary. It is a rank-2 tensor with reducible parts in general. To decompose the graviton tensor $h_{\mu\nu}$ to its transverse and traceless part h , and trace-full part f we follow [25] and define

$$h_{\mu\nu} = \epsilon_{\mu\nu}^{TT} h + \tilde{k}^2 \epsilon_{\mu\nu}^T f - \tilde{k}_\mu \tilde{k}_\nu H + \tilde{k}_\mu A_\nu^\perp + \tilde{k}_\nu A_\mu^\perp \quad (\text{IV.21})$$

where

$$\begin{aligned} k^\mu \epsilon_{\mu\nu}^{TT} &= \eta^{\mu\nu} \epsilon_{\mu\nu}^{TT} = 0 \\ \epsilon_{\mu\nu}^T &= \frac{1}{4} \eta_{\mu\nu} \end{aligned} \quad (\text{IV.22})$$

with $\alpha \equiv \tilde{k}/kz_0$ a dimensionless normalization constant which can be fixed empirically. Here z_0 is the hard-wall scale, and $k^\mu A_\mu^\perp = 0$. A similar rescaling follows in the soft-wall model with $z_0 \rightarrow 1/\tilde{\kappa}_V$.

In a gauge where $A_\mu^\perp = 0$, the equation of motion for h decouples. In contrast, the equations for f , H , and φ (denoted as k in [25]) are coupled (see Eqs.7.16-20 in [25]). Diagonalizing the equations, one can show that f satisfies the same equation of motion as h [25]. Also note that $f_0 = f(z=0)$ couples to T_μ^μ of the gauge theory, while $H_0 = H(z=0)$ couples to $k^\mu k^\nu T_{\mu\nu} \equiv 0$ (see Eq.7.6 of [25]).

1. Action

The effective action for the graviton ($\eta_{\mu\nu} \rightarrow \eta_{\mu\nu} + h_{\mu\nu}$) and dilaton fluctuations ($\phi \rightarrow \phi + \varphi$) follows from the Einstein-Hilbert action plus dilaton by expanding to quadratic order, and after adding the background de Donder gauge fixing term. The result is

$$S = \int d^5x \sqrt{g} e^{-2\phi} (\mathcal{L}_{h+f} + \mathcal{L}_\varphi), \quad (\text{IV.23})$$

with

$$\begin{aligned} \mathcal{L}_{h+f} &= -\frac{1}{4\tilde{g}_5^2} g^{\mu\nu} \eta^{\lambda\rho} \eta^{\sigma\tau} \partial_\mu h_{\lambda\sigma} \partial_\nu h_{\rho\tau} \\ &\quad + \frac{1}{8\tilde{g}_5^2} g^{\mu\nu} \eta^{\alpha\beta} \eta^{\gamma\sigma} \partial_\mu h_{\alpha\beta} \partial_\nu h_{\gamma\sigma}, \\ \mathcal{L}_\varphi &= +\frac{1}{2\tilde{g}_5^2} g^{\mu\nu} \partial_\mu \varphi \partial_\nu \varphi, \end{aligned} \quad (\text{IV.24})$$

and $\tilde{g}_5^2 = 2\kappa^2 = 16\pi G_N = 8\pi^2 / N_c^2$.

2. Spectrum

In the soft wall model, the glueball spectrum is determined by solving the equation of motion for $h_{\mu\nu}$ following from (IV.23). The results for the spin-2 glueball masses and decay constants are

$$m_n^2 = 8\tilde{\kappa}_N^2 (n+1) \quad \tilde{g}_5 f_n = 2\tilde{\kappa}_N \quad (\text{IV.25})$$

They differ from their vector meson counterparts in (IV.19) by the replacements $\tilde{\kappa}_V \rightarrow \sqrt{2}\tilde{\kappa}_N$ and $g_5 \rightarrow \tilde{g}_5$

due to the difference in the bulk actions. For spin-0 glueballs, we have for the trace-full part of the metric fluctuation

$$m_n^2 = 8\tilde{\kappa}_N^2(n+1) \quad \sqrt{2}\tilde{g}_5 f_n = 2\tilde{\kappa}_N \quad (\text{IV.26})$$

after replacing $\tilde{g}_5 \rightarrow \sqrt{2}\tilde{g}_5$ in the results for spin-2 glueballs. For the dilaton fluctuations we have

$$m_n^2 = 8\tilde{\kappa}_N^2(n+1) \quad \tilde{g}_5 f_n = 2\tilde{\kappa}_N \quad (\text{IV.27})$$

3. Couplings

For the graviton in the axial gauge $h_{\mu z} = h_{zz} = 0$. The pertinent couplings in Fig. 2, which follow from linearizing the action (IV.15) by replacing $\eta_{\mu\nu} \rightarrow \eta_{\mu\nu} + h_{\mu\nu}$, are

$$\begin{aligned} h\bar{\Psi}\Psi : & \quad -\frac{\sqrt{2\kappa^2}}{2} \int d^5x \sqrt{g} h_{\mu\nu} T_F^{\mu\nu} \\ hAA : & \quad -\frac{\sqrt{2\kappa^2}}{2} \int d^5x \sqrt{g} h_{\mu\nu} T_V^{\mu\nu} \end{aligned} \quad (\text{IV.28})$$

with the energy-momentum tensors

$$\begin{aligned} T_F^{\mu\nu} &= e^{-\phi} \frac{i}{2} z \bar{\Psi} \gamma^\mu \overset{\leftrightarrow}{\partial}^\nu \Psi - \eta^{\mu\nu} \mathcal{L}_F, \\ T_V^{\mu\nu} &= -e^{-\phi} \left(z^A \eta^{\rho\sigma} \eta^{\mu\beta} \eta^{\nu\gamma} F_{\beta\rho}^V F_{\gamma\sigma}^V \right. \\ &\quad \left. - z^A \eta^{\mu\beta} \eta^{\nu\gamma} F_{\beta z}^V F_{\gamma z}^V \right) - \eta^{\mu\nu} \mathcal{L}_V. \end{aligned} \quad (\text{IV.29})$$

Note that the UV-boundary term in the (IV.15) vanishes for the normalizable modes of the fermion. For the dilaton the couplings are

$$\begin{aligned} \varphi\bar{\Psi}\Psi : & \quad \sqrt{2\kappa^2} \int d^5x \sqrt{g} \frac{e^{-\phi}}{2} \left(\frac{z}{2} \partial_z \varphi \right) \bar{\Psi} \gamma^5 \Psi + \sqrt{2\kappa^2} \int d^5x \sqrt{g} \frac{e^{-\phi}}{2} \left(\frac{iz}{2} \partial_\mu \varphi \right) \bar{\Psi} \gamma^\mu \Psi \\ \varphi AA : & \quad \sqrt{2\kappa^2} \int d^5x \sqrt{g} e^{-\phi} (-\varphi) \left(-\frac{1}{4} g^{\mu\alpha} g^{\beta\nu} F_{\mu\nu}^V F_{\alpha\beta}^V \right) \end{aligned} \quad (\text{IV.30})$$

We have canonically normalized the bulk fields through the substitutions

$$\Psi \rightarrow g_5 \Psi \quad V_N \rightarrow g_5 V_N \quad \varphi \rightarrow \sqrt{2\kappa^2} \varphi \quad h_{\mu\nu} \rightarrow \sqrt{2\kappa^2} h_{\mu\nu} \quad (\text{IV.31})$$

which makes the couplings and power counting manifest in Witten diagrams. Note that after this rescaling, the meson decay constants in (IV.19) and the glueball decay constants in (IV.25-IV.27) redefine through $g_5 f_n \rightarrow f_n$. This will be understood in most of our analysis.

Evaluating the couplings or the vertices (IV.28)-(IV.30) on the solutions, Fourier transforming the fields to momentum space, and integrating by part the trace-full part for the fermions, we find for the couplings to the fermions ($h\bar{\Psi}\Psi$) and gauge fields (hAA)

$$\begin{aligned} h\bar{\Psi}\Psi : & \quad \int \frac{d^4 p_2 d^4 p_1 d^4 k}{(2\pi)^{12}} (2\pi)^4 \delta^4(p_2 - k - p_1) \\ & \quad \times (S_{h\bar{\Psi}\Psi}^k + S_{f\bar{\Psi}\Psi}^k) \\ hAA : & \quad \int \frac{d^4 q' d^4 q d^4 k}{(2\pi)^{12}} (2\pi)^4 \delta^4(q' - k - q) \\ & \quad \times (S_{hAA}^k + S_{fAA}^k) \end{aligned} \quad (\text{IV.32})$$

The corresponding couplings to the dilatons are

with

$$\begin{aligned}\varphi_{\bar{\Psi}\Psi} &: \int \frac{d^4 p_2 d^4 p_1 d^4 k}{(2\pi)^{12}} (2\pi)^4 \delta^4(p_2 - k - p_1) S_{\varphi_{\bar{\Psi}\Psi}}^k \\ \varphi_{AA} &: \int \frac{d^4 q' d^4 q d^4 k}{(2\pi)^{12}} (2\pi)^4 \delta^4(q' - k - q) S_{\varphi_{AA}}^k\end{aligned}\tag{IV.33}$$

$$\begin{aligned}S_{h_{\bar{\Psi}\Psi}}^k &= -\frac{\sqrt{2\kappa^2}}{2} \int dz \sqrt{g} e^{-\phi} z \epsilon_{\mu\nu}^{TT} h(k, z) \bar{\Psi}(p_2, z) \gamma^\mu p^\nu \Psi(p_1, z), \\ S_{f_{\bar{\Psi}\Psi}}^k &= -\frac{\sqrt{2\kappa^2}}{2} \int dz \sqrt{g} e^{-\phi} z \bar{\Psi}(p_2, z) \left(\epsilon_{\mu\nu}^T f(k, z) \tilde{k}^2 \gamma^\mu p^\nu + \partial_z (\epsilon_{\mu\nu}^T f(k, z)) k^2 \eta^{\mu\nu} \gamma^5 + \epsilon_{\mu\nu}^T f(k, z) \tilde{k}^2 \eta^{\mu\nu} k_\alpha \gamma^\alpha \right) \Psi(p_1, z), \\ S_{h_{AA}}^k &= \sqrt{2\kappa^2} \int dz \sqrt{g} e^{-\phi} z^4 \epsilon_{\mu\nu}^{TT} h(k, z) K^{\mu\nu}(q, q', n, n', z), \\ S_{f_{AA}}^k &= \frac{\sqrt{2\kappa^2}}{2} \int dz \sqrt{g} e^{-\phi} z^4 \epsilon_{\mu\nu}^T f(k, z) \tilde{k}^2 \left(K^{\mu\nu}(q, q', n, n', z) - \frac{1}{4} \eta^{\mu\nu} K(q, q', n, n', z) \right),\end{aligned}\tag{IV.34}$$

and

$$\begin{aligned}S_{\varphi_{\bar{\Psi}\Psi}}^k &= \frac{\sqrt{2\kappa^2}}{2} \int dz \sqrt{g} e^{-\phi} z \bar{\Psi}(p_2, z) \left(\partial_z \varphi(k, z) \gamma^5 + \varphi(k, z) k_\alpha \gamma^\alpha \right) \Psi(p_1, z), \\ S_{\varphi_{AA}}^k &= \frac{\sqrt{2\kappa^2}}{4} \int dz \sqrt{g} e^{-\phi} z^4 \varphi(k, z) K(q, q', n, n', z),\end{aligned}\tag{IV.35}$$

We have set $q^2 = -Q^2$, $q'^2 = -Q'^2$ for space-like momenta, and defined

$$\begin{aligned}K^{\mu\nu}(q, q', n, n', z) &\equiv B_1^{\mu\nu} \mathcal{V}(Q, z) \mathcal{V}(Q', z) - B_0^{\mu\nu} \partial_z \mathcal{V}(Q, z) \partial_z \mathcal{V}(Q', z), \\ B_0^{\mu\nu}(n, n') &\equiv n^\mu n'^\nu, \\ B_1^{\mu\nu}(q, q', n, n') &\equiv n \cdot n' q^\mu q'^\nu - q \cdot n' n^\mu q'^\nu - q' \cdot n q^\mu n'^\nu + q \cdot q' n^\mu n'^\nu.\end{aligned}\tag{IV.36}$$

with $B_{1,0} = \eta_{\mu\nu} B_{1,0}^{\mu\nu}$, and $K = \eta_{\mu\nu} K^{\mu\nu}$. The non-normalizable wave function for the virtual photon $\mathcal{V}(Q, z)$ is given in Appendix XII.

V. GRAVITATIONAL FORM FACTORS

The graviton coupling to the Dirac fermion in bulk is through its energy momentum tensor. In the conformally broken geometry (hard or soft wall), the corresponding energy momentum tensor traces to the normalization of the bulk Dirac fermion as a nucleon state, modulo the source field normalization at the boundary (see below). More importantly, since the holographic construction operates in the limit of a large number of colors, it follows that the energy momentum tensor of the bulk Dirac

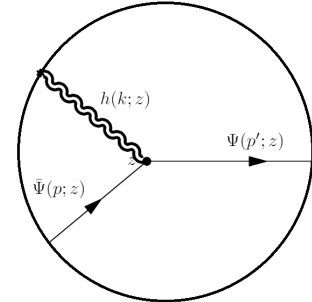


FIG. 3: Witten diagram for the gravitational form factor $A(t)$ due to the exchange of spin-2 glueball resonances.

fermion is dual to the quenched energy momentum tensor of the nucleon. In other words, only the gluonic con-

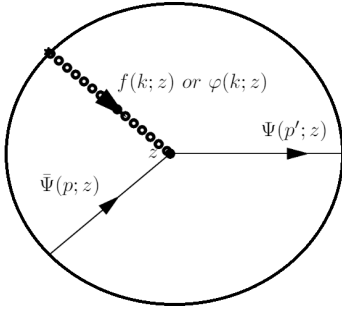


FIG. 4: Witten diagram for the gravitational form factor $C(t)$ due to the exchange of scalar glueball resonances from the trace-full part of the metric fluctuation $f(k, z)$. Also shown is a form factor due to the exchange of the dilatonic scalar glueball resonances $\varphi(k, z)$.

tribution to the energy momentum tensor is picked by the photoproduction amplitude close to threshold in the present holographic analysis.

More specifically, the energy momentum tensor to the bulk Dirac fermion involves both the 2^{++} tensor glueball field h and the 0^{++} scalar glueball field f , see Fig. 3 and 4,

$$i \langle p_2 | T^{\mu\nu}(0) | p_1 \rangle = (-i) V_{h\bar{\Psi}\Psi}^{\mu\nu(TT)}(p_1, p_2, K) + (-i) V_{f\bar{\Psi}\Psi}^{\mu\nu(T)}(p_1, p_2, K), \quad (\text{V.37})$$

with the explicit vertices

$$\begin{aligned} V_{h\bar{\Psi}\Psi}^{\mu\nu(TT)}(p_1, p_2, K) &= -\frac{1}{2g_5^2} \int dz \sqrt{g} e^{-\phi} z \bar{\Psi}(p_2, z) \gamma^\mu p^\nu \Psi(p_1, z) \mathcal{H}(K, z) \\ &= -\frac{1}{2g_5^2} \int dz \sqrt{g} e^{-\phi} z (\psi_R^2(z) + \psi_L^2(z)) \mathcal{H}(K, z) \times \bar{u}(p_2) \gamma^\mu p^\nu u(p_1), \\ V_{f\bar{\Psi}\Psi}^{\mu\nu(T)}(p_1, p_2, K) &= -\frac{1}{2g_5^2} \int dz \sqrt{g} e^{-\phi} z (\psi_L(z) \psi_R(z) - \psi_R(z) \psi_L(z)) \partial_z \mathcal{F}(K, z) \times \tilde{k}^2 \eta^{\mu\nu} \times \bar{u}(p_2) u(p_1) \\ &\quad - \frac{1}{16g_5^2} \int dz \sqrt{g} e^{-\phi} z (\psi_R^2(z) + \psi_L^2(z)) \mathcal{F}(K, z) \times \tilde{k}^2 \eta^{\mu\nu} \times \bar{u}(p_2) (\gamma_\alpha p^\alpha + 4k_\alpha \gamma^\alpha) u(p_1). \end{aligned} \quad (\text{V.38})$$

They follow by substituting the normalizable mode $J_h(m_n, z)$ and $J_f(m_n, z)$ by the non-normalizable mode $\mathcal{H}(K, z)$ (given in XIII.139) and $\mathcal{F}(K, z)$ (given in XIII.157) in the second vertices of (XIV.179) and (XIV.179) for space like momenta $k^2 = -K^2$, with the boundary value for the source set generically to $\mathcal{H}(K, 0) = 1$. Below, we show that this boundary condi-

tion is tied to the normalization of the (gluonic) trace of the energy momentum tensor in the bulk Dirac fermion state as a nucleon and will relax it, since it is arbitrary in holography.

With this in mind, a comparison of (V.37-V.39) to the standard decomposition of the energy-momentum form factor

$$\langle p_2 | T^{\mu\nu}(0) | p_1 \rangle = \bar{u}(p_2) \left(A(k) \gamma^{(\mu} p^{\nu)} + B(k) \frac{i p^{(\mu} \sigma^{\nu)\alpha} k_\alpha}{2m_N} + C(k) \frac{k^\mu k^\nu - \eta^{\mu\nu} k^2}{m_N} \right) u(p_1), \quad (\text{V.39})$$

yields

$$A(K) = -\frac{C(K)}{(\alpha z_0 m_N / 2)^2} = \frac{1}{2g_5^2} \int dz \sqrt{g} e^{-\phi} z (\psi_R^2(z) + \psi_L^2(z)) \mathcal{H}(K, z). \quad (\text{V.40})$$

For the soft wall model,

$$A(K) = A(0) (a_K + 1) \left(- (1 + a_K + 2a_K^2) + 2 (a_K + 2a_K^3) \Phi(-1, 1, a_K) \right), \quad (\text{V.41})$$

or equivalently

$$A(K) = A(0) \left((1 - 2a_K)(1 + a_K^2) + a_K(1 + a_K)(1 + 2a_K^2) \left(\psi\left(\frac{1 + a_K}{2}\right) - \psi\left(\frac{a_K}{2}\right) \right) \right) \quad (\text{V.42})$$

with $a_K = K^2/8\tilde{\kappa}_N^2$. Here $\Phi(-1, 1, a')$ refers to the LerchPhi function, and $\psi(x)$ refers to the digamma function or harmonic number $H_x = \psi(x) + \gamma$. Modulo $A(0)$, (V.41) is in agreement with the result in [21]. The gravitational form factor $C(K)$ is proportional to $A(K)$ modulo a negative overall constant $-(\alpha z_0 m_N/2)^2 < 0$ which is left undetermined since α is arbitrary in the tensor decomposition (IV.21). We note that (V.37) gives $\langle p | T_\mu^\mu | p \rangle = 2A(0)m_N^2$. Since the boundary value $\mathcal{H}(K, 0) = \mathcal{H}(0, z)$ is arbitrary as we just noted above, it follows that $A(0)$ is not fixed in holography. This will be understood from here on.

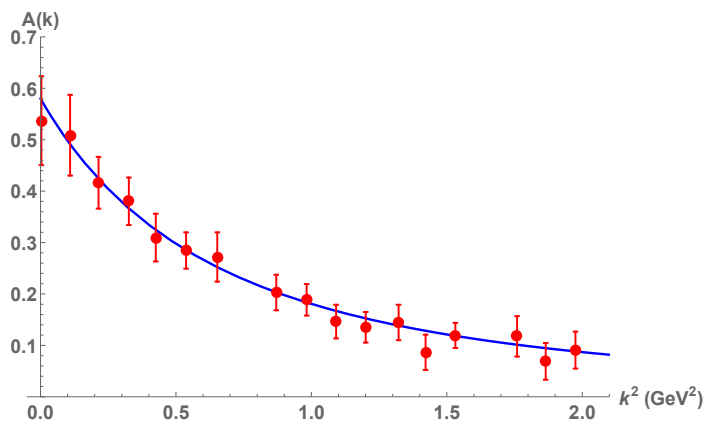


FIG. 5: Holographic gravitational form factor $A(k)$ (for $k^2 \geq 0$) shown in solid-blue curve versus the lattice data in red-squares [26].

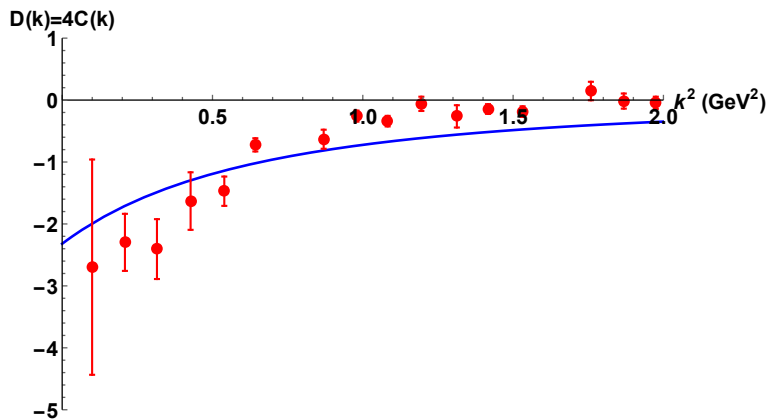


FIG. 6: Holographic gravitational form factor $D(k) = 4C(k)$ (for $k^2 \geq 0$) shown in solid-blue curve versus the lattice data in red-squares [26].

The invariant form factors $A(k), B(k), C(k)$ (for $k^2 \geq 0$) measure the gluonic content of the energy momentum tensor in the nucleon state, as the holographic dual of

the energy momentum tensor of the dilation in bulk in the double limit of large N_c, λ . This limit maps the bulk fields in a soft or hard wall metric, to a pure Yang-Mills

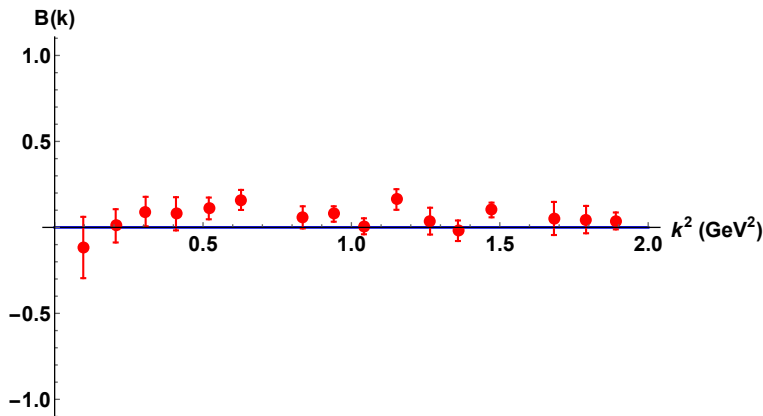


FIG. 7: Holographic gravitational form factor $B(k) = 0$ (for $k^2 \geq 0$) shown in solid-blue curve versus the lattice data in red-squares [26].

theory at the boundary in the confining regime. More specifically, the form factor $A(k)$ through $\mathcal{H}(K, z)$ in bulk resums the 2^{++} or tensor glueball Regge trajectory as given in (XIII.139). For the soft wall model, the result is in agreement with the one reported in [21]. The form factor $C(k)$ through $\mathcal{F}(K, z)$ in bulk resums the 0^{++} or scalar glueball Regge trajectory as shown in (XIII.157). In holography, the scalar and tensor glueball spectra are degenerate as we noted earlier (same bulk equations for h, f), so $\mathcal{H}(K, z)$ and $\mathcal{F}(K, z)$ are tied, i.e $\mathcal{F} = -2\mathcal{H}$. The factor of 2 reflects on the $\frac{1}{2}$ difference in the normalization of the kinetic energies in (IV.24). Finally, the Pauli-like form factor $B(k) = 0$ as the coupling of the graviton to the bulk Dirac fermion through the spin-connection in (IV.16) vanishes,

$$\frac{1}{8}\omega_{NAB}\bar{\Psi}e_C^N\Gamma^C\frac{i}{2}[\Gamma^A,\Gamma^B]\Psi\rightarrow\frac{i}{8}h_\alpha^\mu\bar{\Psi}\Gamma^\alpha[\Gamma_\mu,\Gamma^z]\Psi=0 \quad (\text{V.43})$$

The soft wall results for the gravitational form factor $A(k)$ compares well with the recently reported lattice results, as shown in Fig. 5. The solid-blue curve is our result for the soft wall model, and the red-squares are the recent lattice data [26]. The re-summed $A(k)$ (for $k^2 \geq 0$) in the soft wall model is well reproduced by the dipole form factor

$$A(k)=\frac{A(0)}{\left(1+\frac{k^2}{m_A^2}\right)^2} \quad (\text{V.44})$$

with $m_A = 1.124$ GeV in comparison to the reported lat-

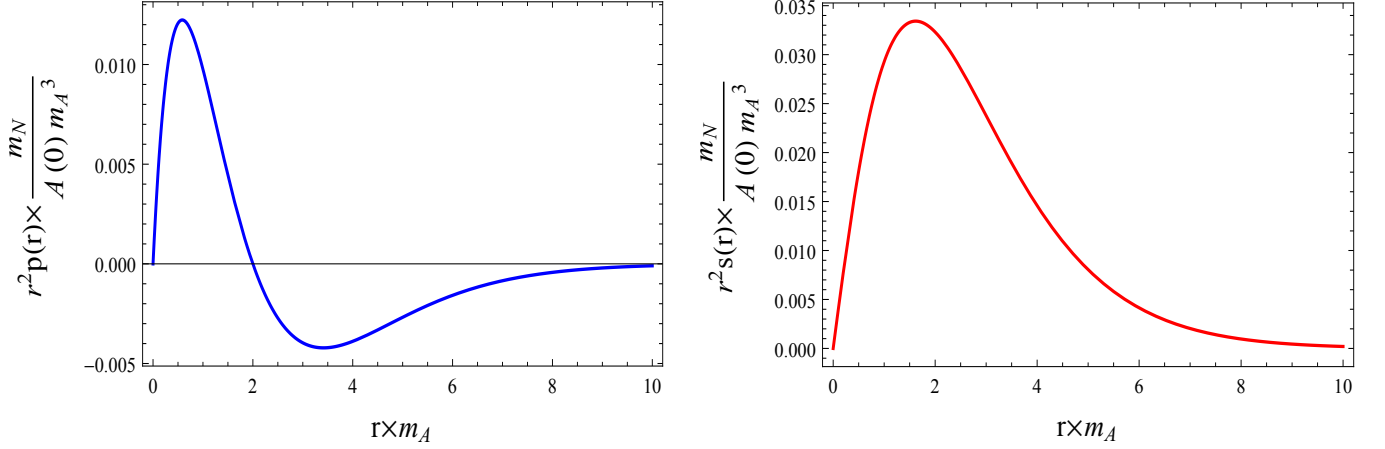
tice value $m_{A,\text{lattice}} = 1.13$ GeV. The arbitrary normalization $A(0) = 0.58$ was adjusted to the lattice data [26]. Recall that the gravitational form factor $A(k)$ is saturated by the 2^{++} glueball trajectory without any quark mixing, essentially a quenched result. In Fig. 6 we show in the solid-blue curve the holographic gravitational form factor $D(k) \equiv 4C(k) = -4A(k)$ with $\alpha = 2/(z_0 m_N)$ in the soft wall model, versus the reported lattice results in red-squares [26]. In holography $C(k)$ is saturated by the 0^{++} massive glueballs which are degenerate with the 2^{++} ones, hence $m_A = 1.124$ GeV in comparison to $m_A = 0.48$ GeV from the lattice. The difference is likely due to the strong scalar-isoscalar quark mixing to the 0^{++} glueball channel in the unquenched lattice simulations, in particular to the light sigma meson with a mass of about 0.5 GeV. In Fig. 7 we show the lattice results in red-squares for $B(k)$ which are consistent with $B(k) = 0$ in holography shown as a solid-blue curve.

VI. HOLOGRAPHIC PRESSURE AND SHEAR INSIDE THE PROTON

Using the dipole representation for $A(K)$ (V.44) which is a good parametrization of our holographic results, the D-term as $D(K) = -4A(K)$ can be written as

$$D(K)=\frac{-4A(0)}{\left(1+\frac{K^2}{m_A^2}\right)^2} \quad (\text{VI.45})$$

with $m_A = 1.124$ GeV. The Fourier transform (VI.45) of the three-dimensional coordinate space gives ($E = m_N$)



(a) The pressure distribution inside the proton (VI.47) for soft-wall holographic QCD with $m_A = 1.124$ GeV.

(b) The shear force inside the proton (VI.47) for soft-wall holographic QCD with $m_A = 1.124$ GeV.

FIG. 8: Holographic pressure and shear inside the proton.

$$\tilde{D}(r) = -4A(0) \int \frac{d^3 K}{2E(2\pi)^3} \frac{e^{-iK \cdot r}}{\left(1 + \frac{K^2}{m_A^2}\right)^2} = -A(0) \frac{m_A^3}{4\pi m_N} e^{-m_A r}, \quad (\text{VI.46})$$

The holographic shear $s(r)$ and pressure $p(r)$ distributions in the proton can be expressed in terms of $\tilde{D}(r)$ as [27]

$$\begin{aligned} s(r) &= -\frac{r}{2} \frac{d}{dr} \frac{1}{r} \frac{d}{dr} \tilde{D}(r) \\ p(r) &= \frac{1}{3} \frac{1}{r^2} \frac{d}{dr} r^2 \frac{d}{dr} \tilde{D}(r) \end{aligned} \quad (\text{VI.47})$$

In Fig. 8a,b we show the holographic gluon contribution to the pressure $p(r)$ distribution and shear force $s(r)$, respectively. The results are in agreement with the lattice QCD result [28] for the gluon contribution. They are also comparable to the experimentally extracted quark contributions in [29]. Below, we will argue that the holographic relationship $D(K) = -4A(K)$ will allow the extraction of the pressure and shear of the proton from the

threshold photoproduction data of heavy vector mesons $V = J/\Psi, \Upsilon$.

VII. HOLOGRAPHIC VECTOR MESON DOMINANCE

The diffractive scattering amplitude with a single graviton and dilaton exchanges is detailed in Appendix XIII. For photoproduction or electroproduction close to the photon point $Q^2 = 0$, and we may set $\mathcal{V}(Q = 0, z) = 1$ in \mathcal{V}_{hAA} in (XIV.182). This will be indicated by the re-labeling of the entry photon $A \rightarrow \gamma$. This will be understood in the remainder of our analysis. With this in mind, The combined amplitudes (XIV.177) read

$$\begin{aligned} -\mathcal{A}_{\gamma p \rightarrow A p}(s, t) &= \mathcal{A}_{\gamma p \rightarrow A p}^{\varphi}(s, t) + \mathcal{A}_{\gamma p \rightarrow A p}^h(s, t) + \mathcal{A}_{\gamma p \rightarrow A p}^f(s, t) \\ &= \frac{1}{2g_5^4} \mathcal{V}_{hAA} B_{\alpha\beta}^1 \mathcal{V}_{h\Psi\Psi}^{\alpha\beta(TT)} + \frac{1}{g_5^4} \mathcal{V}_{fAA} B^1 \mathcal{V}_{f\Psi\Psi}^{(T)} + \frac{1}{g_5^4} \tilde{\mathcal{V}}_{\varphi AA} B^1 \mathcal{V}_{\varphi\Psi\Psi}, \end{aligned} \quad (\text{VII.48})$$

The effective vertices for the hard-wall model are

$$\begin{aligned} \mathcal{V}_{hAA} &= \frac{\sqrt{2\kappa^2}}{2} \int_0^{z_0} dz \sqrt{g} z^4 \mathcal{V}(Q', z) \frac{z^4}{4}, \\ \mathcal{V}_{fAA} &= \eta_{\mu\nu} \mathcal{V}_{fAA}^{\mu\nu(T)} = 0, \end{aligned} \quad (\text{VII.49})$$

$$\begin{aligned} \tilde{\mathcal{V}}_{\varphi AA} &= \frac{\sqrt{2\kappa^2}}{4} \int_0^{z_0} dz \sqrt{g} z^4 \mathcal{V}(Q', z) \frac{z^4}{4}, \\ \mathcal{V}_{\varphi\Psi\Psi} &= 0. \end{aligned} \quad (\text{VII.50})$$

The corresponding vertices for the soft wall model follows through the substitution $\sqrt{g} \rightarrow \sqrt{g}e^{-\tilde{\kappa}_V^2 z^2}$ with $\tilde{\kappa}_V$ the soft wall scale. $B_{\alpha\beta}^1$ and $B^1 = \eta^{\mu\nu} B_{\mu\nu}^1$ are defined in (IV.36).

The TT-part of the transverse and traceless 2^{++} glueball contribution corresponds to $\alpha, \beta = x, y$. The T-coupling of the transverse and traceful 0^{++} glueball to the virtual photons involves the full photon energy momentum tensor and vanishes after contraction with $\epsilon_{\mu\nu}^T$. The TT-coupling involves only the non-trace part of the

photon energy momentum tensor and does not vanish after contraction with $\epsilon_{\mu\nu}^{TT}$. The Yukawa coupling of the dilaton to the bulk Dirac fermion is null as we noted earlier. As a result, the scattering amplitude (VII.48) is solely due to the exchange of the 2^{++} glueball.

The result (VII.48-VII.50) is for a general bulk-to-boundary current $\mathcal{V}(Q', z)$ which sums over a tower of vector meson resonances. The production of a specific meson at the boundary, say charmonium or upsilonium, amounts to the substitution

$$\mathcal{V}(Q', z) \rightarrow \phi_n(z) = c_n z J_1(m_n z) = \frac{f_n}{m_n}(m_n z) J_1(m_n z) \quad (\text{VII.51})$$

in (VII.49-VII.49) with $c_n = \frac{\sqrt{2}}{z_0 J_1(m_n z_0)}$ and f_n the decay constant of a heavy meson of mass m_n , with the identification $n = 0$ for J/Ψ . As a result, the total amplitude for the photoproduction of J/Ψ can be written in the block form

$$\mathcal{A}_{\gamma p \rightarrow J/\Psi p}(s, t) = -\frac{1}{2g_5^4} \mathcal{V}_{hAA} B_{\alpha\beta}^1 \mathcal{V}_{h\Psi\Psi}^{\alpha\beta(TT)}, \quad (\text{VII.52})$$

with the vertices for a hard wall

$$\begin{aligned} V_{h\Psi\Psi}^{\mu\nu(TT)}(p_1, p_2, K) &= -\frac{\sqrt{2\kappa^2}}{2} \int dz \sqrt{g} e^{-\phi} z (\psi_R^2(z) + \psi_L^2(z)) \mathcal{H}(K, z) \times \bar{u}(p_2) \gamma^\mu p^\nu u(p_1), \\ \mathcal{V}_{hAA} &= \left(\frac{f_n}{m_n}\right) \times \frac{\sqrt{2\kappa^2}}{2} \int_0^{z_0} dz \sqrt{g} z^4 \times (m_n z) J_1(m_n z) \times \frac{z^4}{4} \\ &\approx \left(\frac{f_n}{m_n}\right) \times \left(\frac{\sqrt{2\kappa^2}}{16m_n^4} \int_0^{w_0} dw w^5\right) \equiv \left(\frac{f_V}{M_V}\right) \mathbb{V}_{hAA}, \end{aligned} \quad (\text{VII.53})$$

with $w = m_n z$, $w_0 = m_n z_0$. The wave function for the emitted meson near the boundary is $J_1(w) \approx w/2$. In

comparison, the same arguments for the soft wall model give

$$\begin{aligned} \mathcal{V}_{hAA} &= \left(\frac{f_n}{m_n}\right) \times \frac{\sqrt{2\kappa^2}}{2} \int_0^\infty dz \sqrt{g} e^{-z^2 \tilde{\kappa}_V^2} z^4 \times (2\tilde{\kappa}_V^2 z^2) L_n^1(z^2 \tilde{\kappa}_V^2) \times \frac{z^4}{4} \\ &\approx \left(\frac{f_n}{m_n}\right) \times \left(\frac{\sqrt{2\kappa^2}}{2} \frac{L_n^1(0)}{4\tilde{\kappa}_V^4} \int_0^\infty d\xi e^{-\xi^2} \xi^2\right) \equiv \left(\frac{f_V}{M_V}\right) \mathbb{V}_{hAA}, \end{aligned} \quad (\text{VII.54})$$

with $\xi = \tilde{\kappa}_V^2 z^2$ and $\tilde{\kappa}_V$ the soft wall parameter, and $n = 0$.

(VII.53) and (VII.54) embody the general strictures of VMD with the emergence of $f_n/m_n \equiv f_V/M_V$, the ratio of the leptonic decay constant to the mass of the heavy meson emitted, as illustrated in Fig. 2. This result shows that in holographic QCD, the photoproduction amplitude $\gamma p \rightarrow V p$ follows from the **inverse of the diffractive part** of the deeply virtual Compton scattering amplitude $\gamma^* p \rightarrow \gamma p$ through VMD with $\gamma^* \approx (ef_V/M_V)V$.

The triple coupling \mathbb{V}_{hAA} is the coupling of the bulk graviton with wavefunction near the boundary $h \approx z^2 J_2(m_n z) \approx z^4$ (heavy 2^{++} glueball), to a virtual photon near mass shell with $\mathcal{V}(Q \approx 0, z) \rightarrow 1$, and a virtual photon off mass shell with $\mathcal{V}(Q', z) \rightarrow (f_n/m_n) \times (m_n z) J_1(m_n z)$ (hard wall) or $\mathcal{V}(Q', z) \rightarrow (f_n/m_n) \times (2\tilde{\kappa}_V^2 z^2) L_n^1(z^2 \tilde{\kappa}^2)$ (soft wall). The masses and decay constant for the soft wall are given in (IV.19) with the proviso that $g_5 f_n \rightarrow f_n$ following the canonical rescaling (IV.31).

VIII. DIFFERENTIAL CROSS SECTION FOR PHOTOPRODUCTION

Although our analysis for vector meson production applies equally well to both photoproduction and electroproduction, we now specialize to the photoproduction of heavy mesons given the recent experimental interest in extracting the gluon contribution to the proton state from threshold data at current electron machine facilities. With this in mind, the differential cross section for photoproduction of $V = J/\Psi$ can now be constructed from leading spin $j = 0, 2$ glueball exchanges near threshold. The contribution of higher spin- j exchanges and their regeization will follow. The pertinent differential cross section is of the form

$$\left(\frac{d\sigma}{dt}\right) = \frac{e^2}{16\pi(s - m_N^2)^2} \frac{1}{2} \sum_{\text{pol}} \frac{1}{2} \sum_{\text{spin}} \left| \mathcal{A}_{\gamma p \rightarrow J/\Psi p}^h(s, t) \right|^2, \quad (\text{VIII.55})$$

which is dominated by the TT-part of the graviton or 2^{++} glueball exchange as we noted earlier. The first sum over the photon and J/Ψ polarizations is carried out using the identities

$$\begin{aligned} \sum_{s=1,2} n_s^\mu n_s^{*\nu} &= -\eta^{\mu\nu}, \\ \sum_{s'=1,2,3} n_{s'}^\mu n_{s'}^{*\nu} &= -\eta^{\mu\nu} + \frac{q'^\mu q'^\nu}{M_V^2}, \end{aligned} \quad (\text{VIII.56})$$

The second sum is over the initial and final bulk Dirac

fermion as a proton spin

$$\frac{1}{4} \text{Tr} \left((\gamma_\mu p_2^\mu + m_N) (\gamma_\mu p_1^\mu + m_N) \right) = 2K^2 + 8m_N^2 \quad (\text{VIII.57})$$

Carrying explicitly these summations yield the differential cross section for photoproduction of heavy meson in the spin $j = 2$ exchange approximation as

$$\begin{aligned} \left(\frac{d\sigma}{dt}\right) &= \frac{e^2}{64\pi(s - m_N^2)^2} \times \left(\frac{f_V}{M_V}\right)^2 \mathbb{V}_{hAA}^2 \times \frac{\kappa^2}{2g_5^8} \times \frac{g_5^4 A^2(K)}{m_N^2} \times F(s, t = -K^2, M_V, m_N) \times (2K^2 + 8m_N^2), \\ &= \mathcal{N}^2 \times \frac{e^2}{64\pi(s - m_N^2)^2} \times \frac{A^2(K)}{4m_N^2 A^2(0)} \times F(s, t = -K^2, M_V, m_N) \times (2K^2 + 8m_N^2) \end{aligned} \quad (\text{VIII.58})$$

with all vertex insertions following the rescaling (IV.31) are shown explicitly and, in the last line, we have defined the normalization factor \mathcal{N} as

$$\mathcal{N}^2 = \left(\frac{f_V}{M_V}\right)^2 \mathbb{V}_{hAA}^2 \times \frac{2\kappa^2}{g_5^8} \times g_5^4 A^2(0), \quad (\text{VIII.59})$$

where $A(K)$ is the gravitational form factor (V.40), which reduces to (V.41) for the soft wall model. The kinematical function $F(s, t, M_V, m_N)$ follows from the contractions of the various spins emanating from the photon and graviton vertices, and reads

$$\begin{aligned}
F(s, t, M, m) = & \\
& \frac{1}{4096M^2} \left[-9M^{10} + M^8 \left(-32 + 68m^2 + 28s + 37t \right) + 2M^6 \left(256m^4 + 8m^2(32s - 3t) + t(56 - 40s - 29t) \right) + \right. \\
& 2M^4 \left(-136m^6 + 64s^2 - 56s^3 + 8m^4(8 + 27s - 64t) + 3t^2(-24 + 7t) + 4st(-4 + 9t) - 4m^2(6s^2 + 32s(1 + 4t) + \right. \\
& \left. \left. t(-4 + 25t) \right) \right) + M^2 \left(144m^8 + 144s^4 - 192s^2t + 96s^3t - 16s(-4 + t)t^2 + (80 - 13t)t^3 + 96m^6(-6s + 7t) + \right. \\
& 32m^4(27s^2 - 6t - 39st + 8t^2) + 16m^2(-36s^3 + 30s^2t + 24st(1 + 2t) + t^2(-4 + 17t)) \left. \right) - \\
& t(2m^2 - 2s - t) \left(64m^4 + 8m^6 - 8s^3 + 76m^4t - 16t^2 - 90m^2t^2 + t^3 + 4s^2(16 + 6m^2 + 3t) - \right. \\
& \left. \left. 2s(12m^4 + 3t^2 + m^2(64 + 44t)) \right) \right], \tag{VIII.60}
\end{aligned}$$

with $M_V = M$, $m \equiv m_N$, and $V = J/\Psi, \Upsilon$. In the double limit of large N_c, λ , the differential cross section (VIII.58) scales as

$$\frac{d\sigma}{dt} \sim f_V^2 \left(\frac{\kappa^4}{g_5^4} \right) \sim \frac{1}{N_c^0} (\lambda^0 : \text{soft wall}; \lambda^0 : \text{D7 brane}; \lambda^2 : \text{D9 brane};) \tag{VIII.61}$$

since $f_V \sim N_c^0$ after the rescaling (IV.31). It differs from the scaling of the surface exchange in [5], where their bulk Dirac fermion action is not normalized with $1/g_5^2$. For large s , we note that $F(s, t) \sim s^4$ and the differential cross section is seen to grow like s^2 as expected from a 2^{++} glueball exchange as a graviton. The corresponding amplitude is purely real in this limit. These features reflect on the shortcomings of the $j = 2$ exchange and its lack of reggeization at large \sqrt{s} . They will be addressed below.

This notwithstanding, the differential cross section for photoproduction of a heavy meson is proportional to the gravitational form factor $A(K)$ with $A(0)$ the sought after gluonic contribution to the trace of the energy momentum tensor. However, it is folded with various couplings and kinematical factors that makes its extraction at threshold challenging. For the numerical analysis to follow, we will use the soft wall model with a fixed scale $\tilde{\kappa}_N = 0.350$ GeV, $\kappa^2 = 4\pi^2/N_c^2$ as fixed by the normalization of the kinetic part of the gravitational action in (IV.24), and set $1/g_5^2$ through the D7 or D9 brane embeddings. The coupling \mathbb{V}_{hAA} is fixed by setting $V = J/\Psi$ in bulk.

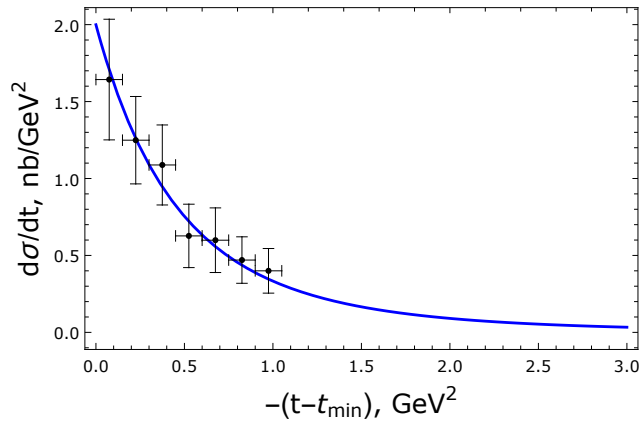


FIG. 9: Differential cross section for $V = J/\Psi$ photoproduction for $E_\gamma = 10.72$ GeV

. The solid-blue curve is our result for the soft-wall model. The data near threshold are from are from GlueX [15].

In Fig. 9, we show the behavior of the differential cross section (VIII.58) for $V = J/\Psi$ photoproduction for a

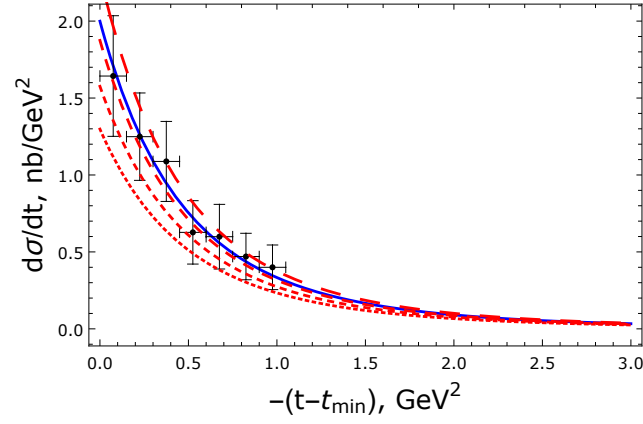


FIG. 10: Same differential cross section for $V = J/\Psi$ photoproduction but different photon energies: $E_\gamma = 11$ GeV large-red-dashing, $E_\gamma = 10.72$ GeV solid-blue-curve, $E_\gamma = 10.6$ GeV medium-red-dashing, $E_\gamma = 10.3$ GeV small-red-dashing, and $E_\gamma = 10$ GeV dotted-red curve. The data are from GlueX [15].

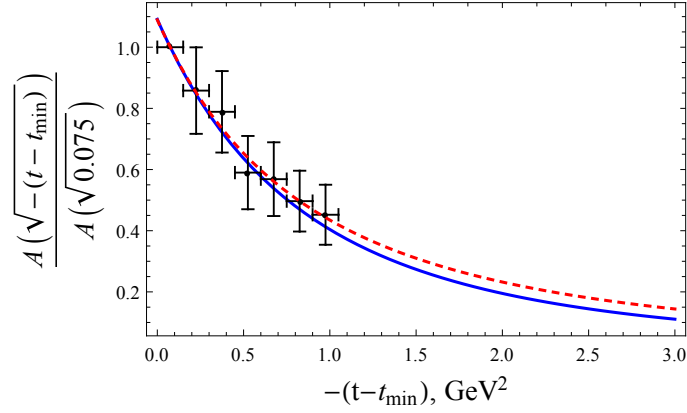


FIG. 11: The gravitational form factor $A(\sqrt{-(t-t_{\min})})$ (normalized by $A(\sqrt{0.075})$) for $\tilde{\kappa}_\rho = 0.350$ GeV, $m_N = 0.94$ GeV, and $m_{J/\psi} = 3.10$ GeV. Blue solid line is our result, and dashed red line is from lattice QCD. We used the data from GlueX [15] with the errors added in quadrature.

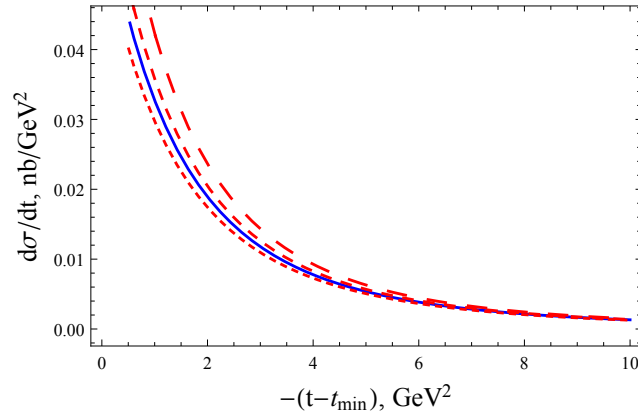


FIG. 12: Differential cross section for $V = \Upsilon$ and different photon energies: $E_\gamma = 58.9$ GeV large-red-dashing, $E_\gamma = 58.6$ GeV medium-red-dashing, $E_\gamma = 58.45$ GeV solid-blue-curve, $E_\gamma = 58.3$ GeV small-red-dashing, and $E_\gamma = 58$ GeV dotted-red curve.

photon energy $E_\gamma = 10.72$ GeV in comparison to the GlueX recent data near threshold [15]. The solid-blue

curve is our result for the soft-wall model. The data near threshold are from GlueX [15]. The mesonic parameters

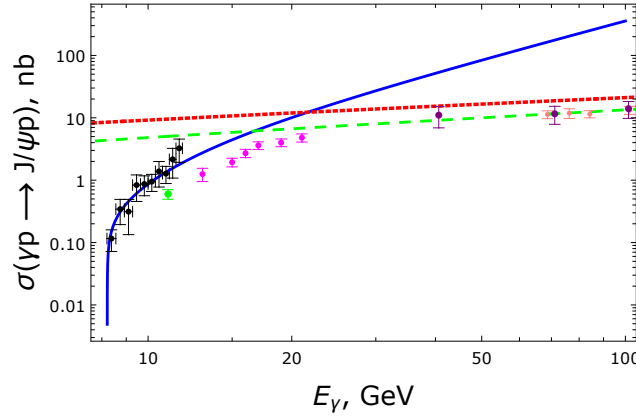


FIG. 13: The total cross section for J/Ψ photoproduction with the same parameters as in Fig. 14, but zoomed in near threshold. The data points are from: GlueX [15] (black), [30] (magenta), [31] (green), [32] (purple), [34] (pink).

were fixed using (IV.19) with $m_0 = M_{J/\psi} = 3.10$ GeV and $f_0 = f_{J/\psi} = 0.405$ GeV for the soft-wall model, and

$$\tilde{\kappa}_V = \frac{2^{3/8} \pi^{3/4} \sqrt{f_V m_V}}{3^{1/4} \lambda^{1/8}} \quad (\text{D9 model})$$

$$\tilde{\kappa}_V = \frac{2^{3/8} \pi^{3/4} \sqrt{f_V m_V}}{3^{1/4} (2^{5/2} \pi)^{1/4}} \quad (\text{D7 model})$$

$$\tilde{\kappa}_V = \frac{2^{3/8} \pi^{3/4} \sqrt{f_V m_V}}{3^{1/4} (2^{5/2} \pi/3)^{1/4}} \quad (\text{Original}) \quad (\text{VIII.62})$$

Here the label 'original' refers the original soft-wall model. The value of the form factor $A(0)$ is model dependent and follows from fitting the normalization factor \mathcal{N} , defined in (VIII.59), to data as

$$\begin{aligned} \mathcal{N} &= \frac{20 \sqrt{\lambda} N_f A(0)}{(10 \tilde{\kappa}_V)^4} = \sqrt{\frac{f_{J/\psi} m_{J/\psi}}{f_V m_V}} \times 7.768 \text{ GeV}^{-4} & (\text{D9 model}) \\ \mathcal{N} &= \frac{20 \cdot 2^{5/2} \pi \times N_f A(0)}{(10 \tilde{\kappa}_V)^4} = \sqrt{\frac{f_{J/\psi} m_{J/\psi}}{f_V m_V}} \times 7.768 \text{ GeV}^{-4} & (\text{D7 model}) \\ \mathcal{N} &= \frac{20 \cdot 2^{5/2} \pi \times N_f A(0)}{3(10 \tilde{\kappa}_V)^4} = \sqrt{\frac{f_{J/\psi} m_{J/\psi}}{f_V m_V}} \times 7.768 \text{ GeV}^{-4} & (\text{Original}). \end{aligned} \quad (\text{VIII.63})$$

In Fig. 10 we show the same differential cross section for other photon energies in dashed-red in comparison to $E_\gamma = 10.72$ GeV in solid-blue and the GlueX recent data [15]. The large-red-dashing curve is for $E_\gamma = 11$ GeV, the medium-red-dashing curve is for $E_\gamma = 10.6$ GeV, the small-red-dashing curve is for $E_\gamma = 10.3$ GeV

and the dotted-red curve is for $E_\gamma = 10$ GeV.

In Fig. 11 we show the empirical ratio of the differential cross sections as a proposal for the ratio of the gravitational form factors $A(\Delta t)/A(\Delta t_{\min})$ with $\Delta t = -(t - t_{\min})^{1/2}$ and $\Delta t_{\min} = \sqrt{0.0075}$ versus Δt^2 in GeV^2 ,

$$\frac{A(\Delta t)}{A(\Delta t_{\min})} = \left(\frac{F(s, t = t_{\min}, M_V, m_N)(-2t_{\min} + 8m_N^2)}{F(s, t = -K^2, M_V, m_N)(2K^2 + 8m_N^2)} \right) \frac{\left(\frac{d\sigma}{dt} \right)}{\left(\frac{d\sigma}{dt} \right)_{\min}} \quad (\text{VIII.64})$$

The blue-solid line is our holographic result (VIII.58), the red-dashed line is the fitted lattice gluonic contribution from the recent simulations in [26], and the data are the ratio of the data from from GlueX [15]. The empirical errors for the ratio have been added in quadrature. (VIII.64) provides for a model independent extraction of the gravitational form factor, under two generic assumptions: 1/ The Yukawa coupling of the dilaton to the bulk Dirac fermion vanishes in holography; 2/ The tensor 2^{++} glueball couplings map on the graviton couplings in bulk.

In Fig. 12 we show the differential cross section for $V = \Upsilon$ production close to threshold for different photon energies which is a prediction, for the same parameter set as the one used for J/Ψ production. The photon energies are: $E_\gamma = 58.9$ GeV large-red-dashing, $E_\gamma = 58.6$ GeV medium-red-dashing, $E_\gamma = 58.45$ GeV solid-blue-curve, $E_\gamma = 58.3$ GeV small-red-dashing, and $E_\gamma = 58$ GeV dotted-red curve. We have used $m_0 = M_\Upsilon = 9.460$ GeV, $f_0 = f_\Upsilon = 0.714$ GeV and κ_V as in (VIII.62) for the models with a soft wall. Note that in this case, $A(0)$ is fixed by the same ratios as in (VIII.63) with the numbers rescaled by the factor $(f_{J/\psi} m_{J/\psi} / f_V m_V)$ to correct for the $V = \Upsilon$ parameters.

In Fig. 13 (solid blue line), we show the total cross section for photoproduction of $V = J/\Psi$ versus the photon energy close to threshold. The total cross section follows by integrating the differential cross section in (VIII.58) using the dipole parametrization (X.96) with $k^2 \rightarrow -t$. The comparison is to GlueX data [15] (black ones). All

other holographic parameters are kept unchanged.

IX. REGGEIZED PHOTOPRODUCTION

The differential cross section (VIII.58) grows rapidly as s^2 at large s as expected from the exchange of a graviton as a tensor glueball exchange with spin-2. The physical cross section grows much slower due to the exchange of a Pomeron instead. The transmutation from a graviton to a Pomeron was originally discussed in [8]. With increasing \sqrt{s} , higher spin- j exchanges contribute leading to a reggeized amplitude with the emergence of a Pomeron. In this section and in supportive material given in the Appendices, we detail the spin- j contribution to (VIII.58) and then re-sum these exchanges to extend the photoproduction results to all \sqrt{s} .

A. Spin- j amplitude

The spin- j exchange amplitude follows from the same considerations as the spin-2 exchange given earlier. Here we summarise the results for the soft wall model with more details given in Appendix XIII together with the results for the hard wall model. With this in mind, the spin- j glueball contribution to the TT-part of the photoproduction amplitude $\gamma p \rightarrow A p$ with an arbitrary virtual photon A , reads

$$i\mathcal{A}_{\gamma p \rightarrow A p}^h(j, s, t) \approx (-i)\mathcal{V}_{hAA}^{\mu\nu(TT)}(j, q_1, q_2, k_z) \times \left(\frac{i}{2}\eta_{\mu\alpha}\eta_{\nu\beta} \right) \times (-i)\mathcal{V}_{h\bar{\Psi}\Psi}^{\alpha\beta(TT)}(j, p_1, p_2, k_z), \quad (\text{IX.65})$$

The explicit form of the tensor TT-vertices \mathcal{V}^{TT} depend on the model used. For the soft-wall model, the normalized wave functions and bulk-to-bulk propagator are

detailed in Appendix XII. The result for the spin- j contribution to the vertices is

$$\begin{aligned}
\mathcal{V}_{hAA}^{\mu\nu(TT)}(j, q_1, q_2, k_z) &= \frac{\sqrt{2\kappa^2}}{2} \int dz \sqrt{g} e^{-\phi} z^{4+2(j-2)} K^{\mu\nu}(q, q', n, n', z) \times C(j) \times z^{\Delta(j)-j-2} \\
\mathcal{V}_{h\bar{\Psi}\Psi}^{\alpha\beta(TT)}(j, p_1, p_2, k_z) &= -\frac{\sqrt{2\kappa^2}}{2} \int dz \sqrt{g} e^{-\phi} z^{1+2(j-2)} \bar{\Psi}(p_2, z) \gamma^\alpha p^\beta \Psi(p_1, z) z^{-(j-2)} \mathcal{H}(j, K, z) \\
&= -\frac{\sqrt{2\kappa^2}}{2} \int dz \sqrt{g} e^{-\phi} z^{1+2(j-2)} (\psi_R^2(z) + \psi_L^2(z)) z^{-(j-2)} \mathcal{H}(j, K, z) \times \bar{u}(p_2) \gamma^\alpha p^\beta u(p_1) \\
&= -\sqrt{2\kappa^2} \times g_5^2 A(j, K) \times \bar{u}(p_2) \gamma^\alpha p^\beta u(p_1), \tag{IX.66}
\end{aligned}$$

with the parameters

$$\begin{aligned}
C(j) &= \tilde{\kappa}_V^{2\Delta(j)-4} \times \frac{1}{\Delta(j)} \frac{2^{\Delta(j)-2} \Gamma(a_K + \frac{\Delta(j)}{2})}{\Gamma(\Delta(j) - 2)} \\
\Delta(j) &= 2 + \sqrt{2\sqrt{\lambda}(j - j_0)} \quad \text{and} \quad a_K = \frac{a}{2} = \frac{K^2}{8\tilde{\kappa}^2} \quad \text{and} \quad j_0 = 2 - \frac{2}{\sqrt{\lambda}} \tag{IX.67}
\end{aligned}$$

For completeness, the analogue vertex $\mathcal{V}_{hAA}^{\mu\nu(TT)}$ for the hard wall model is

$$\mathcal{V}_{hAA}^{\mu\nu(TT)}(j, q_1, q_2, k_z) = \frac{\sqrt{2\kappa^2}}{2} \int dz \sqrt{g} e^{-\phi} z^{4+2(j-2)} K^{\mu\nu}(q, q', n, n', z) \frac{2^{1-\tilde{\Delta}(j)}}{\pi} \times K^{\tilde{\Delta}(j)} \times z^{\tilde{\Delta}(j)+2-(j-2)}{\tilde{\Delta}(j) + 2}, \tag{IX.68}$$

Using (XV.209) in (IX.66), we can write the spin- j form factor $A(j, K)$ of the proton as a bulk Dirac fermion in the soft-wall model as

$$A(j, K) = \frac{1}{2g_5^2} \frac{2^{2-\Delta(j)} \tilde{\kappa}_N^{j-2-\Delta(j)}}{\Gamma(\tilde{a}(j))} \int_0^1 dx x^{\tilde{a}(j)-1} (1-x)^{-\tilde{b}(j)} (I_z^R(x) + I_z^L(x)), \tag{IX.69}$$

with

$$\tilde{a}(j) = a_K + 2 - \frac{1}{2}\Delta(j) \quad \text{and} \quad \tilde{b}(j) = 3 - \Delta(j) \tag{IX.70}$$

The integrals ($\xi = \tilde{\kappa}_N^2 z^2$)

$$I_z^{R/L}(x) = \int dz \sqrt{g} e^{-\phi} z^{1+2(j-2)} \psi_{R/L}^2(z) \xi^{-\frac{(j-2)}{2}} \xi^{2-\frac{\Delta(j)}{2}} \exp\left(-\frac{2x\xi}{1-x}\right), \tag{IX.71}$$

are over the wavefunctions of the proton as a Dirac fermion in bulk in the soft-wall model. Specifically, we have

$$\begin{aligned}
\psi_R(z) &= \frac{\tilde{n}_R}{\tilde{\kappa}_N^{\tau-2}} z^{\frac{5}{2}} \xi^{\frac{\tau-2}{2}} L_0^{(\tau-2)}(\xi), \\
\psi_L(z) &= \frac{\tilde{n}_L}{\tilde{\kappa}_N^{\tau-1}} z^{\frac{5}{2}} \xi^{\frac{\tau-1}{2}} L_0^{(\tau-1)}(\xi),
\end{aligned} \tag{IX.72}$$

with the twist parameter $\tau = 7/2 - 1/2 = 3$. Here $L_n^{(\alpha)}(\xi)$ are the generalized Laguerre polynomials, and

$$\tilde{n}_R = \tilde{n}_L \tilde{\kappa}_N^{-1} \sqrt{\tau-1} \quad \tilde{n}_L = \tilde{\kappa}_N^\tau \sqrt{2/\Gamma(\tau)} \tag{IX.73}$$

Using the wave functions, the integrals in (IX.71) can be carried out explicitly, with the results

$$\begin{aligned}
I_z^R(x) &= \frac{1}{2} \times \tilde{\kappa}_N^{-2(j-2)} \times \left(\frac{\tilde{n}_R}{\tilde{\kappa}_N^{\tau-1}} \right)^2 \times \int d\xi \xi^{\frac{j-2}{2} + \tau - \frac{\Delta(j)}{2}} \left(L_0^{(\tau-2)}(\xi) \right)^2 \exp\left(- \left(\frac{1+x}{1-x} \right) \xi \right), \\
I_z^L(x) &= \frac{1}{2} \times \tilde{\kappa}_N^{-2(j-2)} \times \left(\frac{\tilde{n}_L}{\tilde{\kappa}_N^\tau} \right)^2 \times \int d\xi \xi^{\frac{j-2}{2} + \tau - \frac{\Delta(j)}{2} + 1} \left(L_0^{(\tau-1)}(\xi) \right)^2 \exp\left(- \left(\frac{1+x}{1-x} \right) \xi \right),
\end{aligned} \tag{IX.74}$$

where we used $\phi = e^{-\xi}$. Evaluating the integrals in (IX.74) we obtain

$$\begin{aligned}
I_z^R(x) &= \frac{1}{2} \times \tilde{\kappa}_N^{-2(j-2)} \times \left(\frac{\tilde{n}_R}{\tilde{\kappa}_N^{\tau-1}} \right)^2 \times \Gamma\left(\frac{j-2}{2} + \tau - \frac{\Delta(j)}{2} + 1 \right) \times \left(\frac{1+x}{1-x} \right)^{-\frac{j-2}{2} - \tau + \frac{\Delta(j)}{2} - 1}, \\
I_z^L(x) &= \frac{1}{2} \times \tilde{\kappa}_N^{-2(j-2)} \times \left(\frac{\tilde{n}_L}{\tilde{\kappa}_N^\tau} \right)^2 \times \Gamma\left(\frac{j-2}{2} + \tau - \frac{\Delta(j)}{2} + 2 \right) \times \left(\frac{1+x}{1-x} \right)^{-\frac{j-2}{2} - \tau + \frac{\Delta(j)}{2} - 2}.
\end{aligned} \tag{IX.75}$$

Using (IX.75) in (IX.69), the spin- j glueball form factor of the proton becomes

$$\begin{aligned}
A(j, K) &= \frac{1}{4g_5^2} \frac{\tilde{\kappa}_N^{-(j-2) - \Delta(j)}}{\Gamma(\tilde{a}(j))} \int_0^1 dx x^{\tilde{a}(j)-1} (1-x)^{-\tilde{b}(j)} \\
&\quad \times \left(\left(\frac{\tilde{n}_R}{\tilde{\kappa}_N^{\tau-1}} \right)^2 \times \Gamma(c(j)) \left(\frac{1+x}{1-x} \right)^{-c(j)} + \left(\frac{\tilde{n}_L}{\tilde{\kappa}_N^\tau} \right)^2 \times \Gamma(c(j)+1) \left(\frac{1+x}{1-x} \right)^{-(c(j)+1)} \right),
\end{aligned} \tag{IX.76}$$

with $\Delta(j)$ given in (IX.67), $\tilde{a}(j)$, $\tilde{b}(j)$ given in (IX.70) and

$$c(j) = (\tau + 1) + \frac{j-2}{2} - \frac{\Delta(j)}{2} \tag{IX.77}$$

$A(j, K)$ generalizes the gravitational form factor for all $j \geq 2$. Evaluating the integral in (IX.76), we obtain (IX.81). Inserting (IX.81) in (IX.66), (IX.65) becomes

$$\mathcal{A}_{\gamma p \rightarrow J/\Psi p}(j, s, t) = \mathcal{V}_{hAA}(j) \left(-\frac{1}{2} B_1^{\alpha\beta} \bar{u}(p_2) \gamma_\alpha p_\beta u(p_1) \right) \mathcal{V}_{h\bar{\Psi}\Psi}^{(TT)}(j), \tag{IX.78}$$

The spin- j vertices are

$$\begin{aligned}
\mathcal{V}_{h\bar{\Psi}\Psi}^{(TT)}(j) &= -g_5^2 A(j, K), \\
\mathcal{V}_{hAA}(j) &= \left(\frac{f_n}{m_n} \right) \times \left(\frac{\sqrt{2\kappa^2}}{2} \int_0^\infty dz \sqrt{g} e^{-z^2 \tilde{\kappa}_V^2} z^{4+2(j-2)} \times (2\tilde{\kappa}^2 z^2) L_n^1(z^2 \tilde{\kappa}_V^2) \times C(j) \times z^{\Delta(j) - (j-2)} \right) \\
&\approx \left(\frac{f_n}{m_n} \right) \times \left(\frac{\sqrt{2\kappa^2}}{2} \frac{L_n^1(0)}{\Delta(j) \tilde{\kappa}_V^{\Delta(j)+j-2}} \times C(j) \times \left(\int_0^\infty d\xi e^{-\xi^2} \xi^{\frac{\Delta(j)}{2} + \frac{j}{2} - 1} \right) \right) \equiv \left(\frac{f_V}{M_V} \right) \mathbb{V}_{hAA}(j)
\end{aligned} \tag{IX.79}$$

with $B_1^{\alpha\beta}(q, q', n, n')$ defined in (IV.36). The heavy mesons with $n = J/\Psi$, Υ are subsumed. (IX.78) shows how VMD extends to general spin- j exchange in hologra-

phy, with $\mathbb{V}_{hAA}(j)$ reflecting on its coupling to the pair vector-meson-photon in bulk.

B. Reggeized amplitude

is

After summing over all contributions from the spin- j glueballs, the photoproduction amplitude $\mathcal{A}_{\gamma p \rightarrow J/\Psi p}^{tot}(s, t)$

$$\begin{aligned} \mathcal{A}_{\gamma p \rightarrow J/\Psi p}^{tot}(s, t) &= - \int_{\mathbb{C}} \frac{dj}{2\pi i} \left(\frac{s^{j-2} + (-s)^{j-2}}{\sin \pi j} \right) \mathcal{A}_{\gamma p \rightarrow J/\Psi p}(j, s, t) \\ \mathcal{A}_{\gamma p \rightarrow J/\Psi p}(j, s, t) &= \frac{1}{2} \mathcal{V}_{hAA}(j) \times B_1^{\alpha\beta} \times \frac{2\kappa^2}{g_5^4} \times g_5^2 A(j, K) \times \bar{u}(p_2) \gamma_\alpha p_\beta u(p_1), \end{aligned} \quad (\text{IX.80})$$

The contour \mathbb{C} is at the rightmost of the branch-point of $A(j, K)$. The spin- j glueball form factor $A(j, K)$ of the proton as a bulk Dirac fermion is given in (IX.76) for the

soft wall model. The integrals can be carried explicitly, with the result

$$\begin{aligned} A(j, K) &= \frac{\tilde{\kappa}_N^{-(j-2)-\Delta(j)}}{4g_5^2} \frac{\Gamma(c)\Gamma(1-\tilde{b}+c)}{\Gamma(1-\tilde{b}+c+\tilde{a})} \\ &\times \left(\left(\frac{\tilde{n}_R}{\tilde{\kappa}_N^{\tau-1}} \right)^2 {}_2F_1(\tilde{a}, c+1, 1-\tilde{b}+c+\tilde{a}, -1) + \left(\frac{\tilde{n}_L}{\tilde{\kappa}_N^\tau} \right)^2 \frac{c(1-\tilde{b}+c)}{1-\tilde{b}+c+\tilde{a}} {}_2F_1(\tilde{a}+1, c+1, 2-\tilde{b}+c+\tilde{a}, -1) \right). \end{aligned} \quad (\text{IX.81})$$

The parameters are fixed in (IX.67) as

$$\begin{aligned} 1 - \tilde{b} + c &= (\tau - 1) + \frac{j-2}{2} + \frac{\Delta(j)}{2} \\ 1 - \tilde{b} + c + \tilde{a} &= (\tau + 1) + \frac{j-2}{2} + a_K \end{aligned} \quad (\text{IX.82})$$

Note that at $j = 2$, (IX.81) is exactly equal to the spin-2 gravitational form factor (V.41) (times $1/\tilde{\kappa}_V^4$ to compensate for the new normalization we used for the higher spin case).

From (IX.83-IX.81), we determine the single Pomeron amplitude (total amplitude) in momentum space, after wrapping the j -plane contour \mathbb{C} to the left,

$$\mathcal{A}_{\gamma p \rightarrow J/\Psi p}^{tot}(s, t) = -s^{j_0-2} \int_{-\infty}^{j_0} \frac{dj}{\pi} \left(\frac{1 + e^{-i\pi}}{\sin \pi j} \right) s^{j-j_0} \text{Im}[\mathcal{A}_{\gamma p \rightarrow J/\Psi p}(j, s, t)] \quad (\text{IX.83})$$

The imaginary part follows from the discontinuity of the

Γ -function

$$\begin{aligned} \text{Im}[\mathcal{A}_{\gamma p \rightarrow J/\Psi p}(j, s, t)] &\approx \frac{\tilde{\kappa}_N^{-(j-2)-\Delta(j)}}{\tilde{\kappa}_N^{4-\Delta(j)+j-2}} \times \left(\frac{\tilde{\kappa}_N}{\tilde{\kappa}_V} \right)^{4-\Delta(j)+j-2} \times \frac{\sqrt{2\kappa^2}}{g_5^4} \times \\ &\left(\frac{1}{2} \tilde{\kappa}_V^{4-\Delta(j)+j-2} \Gamma(\Delta(j)-2) \mathcal{V}_{hAA}(j) \times B_1^{\alpha\beta} \times \tilde{\kappa}_N^{j-2+\Delta(j)} g_5^2 A(j, K) \bar{u}(p_2) \gamma_\alpha p_\beta u(p_1) \right) \Big|_{j \rightarrow j_0, \Delta(j) \rightarrow 2} \times \text{Im} \left[\frac{1}{\Gamma(\overline{\Delta(j)})} \right] \end{aligned} \quad (\text{IX.84})$$

with the complex argument

$$\tilde{\Delta}(j) = \Delta(j) - 2 = i\sqrt{2\sqrt{\lambda}(j_0 - j)} \equiv iy \quad (\text{IX.85})$$

and $j_0 = 2 - 2/\sqrt{\lambda}$. For $y \rightarrow 0$, we may approximate $1/\Gamma(iy) \approx iy e^{i\gamma y}$, with the Euler-Mascheroni constant

$\gamma = 0.5772156649\dots$. The single Pomeron amplitude (total amplitude) in momentum space (IX.83) can now be cast in block form

$$\mathcal{A}_{\gamma p \rightarrow J/\Psi p}^{tot}(s, t) = I_j(j_0, s) \times G_5(j_0, s, t) \quad (\text{IX.86})$$

with

$$\begin{aligned} I_j(j_0, s) &= -\tilde{s}^{j_0} \int_{-\infty}^{j_0} \frac{dj}{\pi} \left(\frac{1 + e^{-i\pi}}{\sin \pi j} \right) \tilde{s}^{j-j_0} \sin \left[\tilde{\xi} \sqrt{2\sqrt{\lambda}(j_0 - j)} \right] \\ G_5(j_0, s, t) &= \left(\frac{\tilde{\kappa}_N}{\tilde{\kappa}_V} \right)^{4-\Delta(j)+j-2} \times \frac{1}{s^2} \left(\frac{1}{2} \tilde{\kappa}_V^{4-\Delta(j)+j-2} \Gamma(\Delta(j) - 2) \mathcal{V}_{hAA}(j) \times B_1^{\alpha\beta} \times \frac{\sqrt{2\kappa^2}}{g_5^4} \right. \\ &\quad \left. \times \tilde{\kappa}_N^{j-2+\Delta(j)} g_5^2 A(j, K) \bar{u}(p_2) \gamma_\alpha p_\beta u(p_1) \right) \Big|_{j \rightarrow j_0, \Delta(j) \rightarrow 2} \end{aligned} \quad (\text{IX.87})$$

We have set $\tilde{s} \equiv s/\tilde{\kappa}_N^2$, and defined $\tilde{\xi} \equiv \gamma + \pi/2$. We note that the apparent pole in the Gamma-function at the Pomeron intercept, cancels out in the combination $\Gamma(\Delta(j_0) - 2) \mathcal{V}_{hAA}(j_0)$.

In the block form (IX.86), the spin-j integral $I_j(j_0, s)$ is similar to the spin-j integral in [8] (see Eq. 4.19), with the identifications $\mathcal{K}(s, b^\perp, z, z') \leftrightarrow \mathcal{A}_{\gamma p \rightarrow J/\Psi p}^{tot}(s, t)$,

$(zz'/R^4)G_3(j_0, v) \leftrightarrow G_5(j_0, s, t)$, $\xi(v) \leftrightarrow \tilde{\xi}$, and $\hat{s} \leftrightarrow \tilde{s}$. We then follow [8] to evaluate the spin-j integral by closing the j-contour appropriately. In the high energy limit $\sqrt{\lambda}/\tilde{\tau} \rightarrow 0$ ($\tilde{\tau} \equiv \log \tilde{s}$), the single Pomeron contribution to the photoproduction amplitude is

$$\mathcal{A}_{\gamma p \rightarrow J/\Psi p}^{tot}(s, t) \simeq e^{j_0 \tilde{\tau}} \left[(\sqrt{\lambda}/\pi) + i \right] (\sqrt{\lambda}/2\pi)^{1/2} \tilde{\xi} \frac{e^{-\sqrt{\lambda}\tilde{\xi}^2/2\tilde{\tau}}}{\tilde{\tau}^{3/2}} \left(1 + \mathcal{O}\left(\frac{\sqrt{\lambda}}{\tilde{\tau}}\right) \right) \times G_5(j_0, s, t) \quad (\text{IX.88})$$

As expected, the amplitude develops both a real and imaginary part with a ρ -ratio about constant

$$\rho = \frac{\text{Re}[\mathcal{A}_{\gamma p \rightarrow J/\Psi p}^{tot}(s, t=0)]}{\text{Im}[\mathcal{A}_{\gamma p \rightarrow J/\Psi p}^{tot}(s, t=0)]} \simeq \frac{\sqrt{\lambda}}{\pi} \quad (\text{IX.89})$$

The single Pomeron contribution to the total differential cross section is

$$\begin{aligned} \left(\frac{d\sigma}{dt} \right)_{\text{tot}} &= \frac{e^2}{16\pi(s - m_N^2)^2} \frac{1}{2} \sum_{\text{pol}} \frac{1}{2} \sum_{\text{spin}} \left| \mathcal{A}_{\gamma p \rightarrow J/\Psi p}^{tot}(s, t) \right|^2 \\ &\simeq \frac{e^2}{16\pi(s - m_N^2)^2} \times \left(e^{2j_0 \tilde{\tau}} [(\lambda/\pi^2) + 1] (\sqrt{\lambda}/2\pi) \tilde{\xi}^2 \frac{e^{-\sqrt{\lambda}\tilde{\xi}^2/\tilde{\tau}}}{\tilde{\tau}^3} \right) \times \frac{1}{2} \sum_{\text{pol}} \frac{1}{2} \sum_{\text{spin}} \left| G_5(j_0, s, t) \right|^2 \end{aligned} \quad (\text{IX.90})$$

with the polarization-spin average

$$\begin{aligned}
\sum_{\text{pol,spin}} \left| G_5(j_0, s, t) \right|^2 &= \left(\frac{\tilde{\kappa}_N}{\tilde{\kappa}_V} \right)^{2(4-\Delta(j)+j-2)} \\
&\times \left(\frac{f_V}{M_V} \right)^2 \left(\frac{2\kappa^2}{g_5^2} \tilde{\kappa}_V^{2(4-\Delta(j)+j-2)} \Gamma^2(\Delta(j)-2) \mathbb{V}_{hAA}^2(j) \times \tilde{\kappa}_N^{2(j-2+\Delta(j))} \frac{g_5^4 A^2(j, K)}{m_N^2} \right) \Big|_{j \rightarrow j_0, \Delta(j) \rightarrow 2} \\
&\times \frac{F(s, t = -K^2, M_V, m_N)}{s^4} \times (2K^2 + 8m_N^2)
\end{aligned} \tag{IX.91}$$

and $j_0 = 2 - 2/\sqrt{\lambda}$. Note that the resummed spin- j contribution to the gravitational form factor is now fixed by the Pomeron exchange with the form factor $A(K, j_0)$ at large \sqrt{s} . Remarkably, the emerging Pomeron exchange in the soft wall model in (IX.90) which is a new result, bears much in common with the original conformal Pomeron kernel in [8].

The differential cross section rises with twice the conformal Pomeron intercept or $2 \times (1 - 2/\sqrt{\lambda})$, and asymptotes

$$\begin{aligned}
\left(\frac{d\sigma}{dt} \right)_{\text{tot}} &\sim s^{2-\frac{4}{\sqrt{\lambda}}} \times \left(1 + \frac{\pi^2}{\lambda} \right) \\
&\times \left(\left(\frac{\sqrt{\lambda}}{\log \tilde{s}} \right)^3 + \mathcal{O} \left(\left(\frac{\sqrt{\lambda}}{\log \tilde{s}} \right)^4 \right) \right)
\end{aligned} \tag{IX.92}$$

in the high energy limit with $\log \tilde{s} = \log(s/\tilde{\kappa}_V^2) \gg \sqrt{\lambda}$. Using the optical theorem one can determine the total cross section $\sigma_V(s)$ for $\gamma p \rightarrow V p$ with $V = J/\Psi, \Upsilon$ to be

$$\sigma_V(s) = \left(\frac{16\pi}{1 + \rho^2} \left(\frac{d\sigma}{dt} \right)_{\text{tot}} \Big|_{t=0} \right)^{\frac{1}{2}} \tag{IX.93}$$

with the Pomeron rise $\sigma_V(s) \sim s^{1-2/\sqrt{\lambda}}$ at large \sqrt{s} [8]. Recall that close to threshold, the t-exchange is kinematically bounded as shown in Fig. 1, and the total cross section follows from the differential cross section (VIII.58) by integration using (II.7).

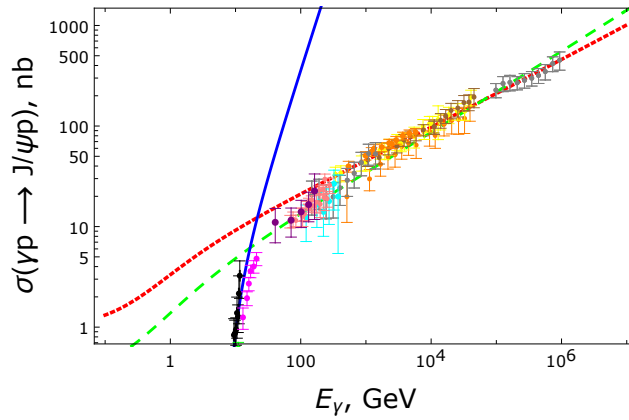


FIG. 14: Total cross section for photoproduction of charmonium with $V = J/\Psi$, from close to threshold to very high energy. The solid (blue) curve is the low-energy regime compared to the data from GlueX [15] (black). The red (tiny dashed) is the high energy regime. The green line (medium dashed) is found after fixing a normalization constant with one high energy data point but with the same high energy 't Hooft coupling constant $\lambda = 11.243$ as the red (tiny dashed) one. The data points are from: [30] (magenta), [31] (green), [32] (purple), [33] (orange), [34] (pink), [35] (yellow), [36] (brown), [37] (orange), and [38] (grey).

In Fig. 14, we show the total cross section for photo- production of charmonium with $V = J/\Psi$ from thresh-

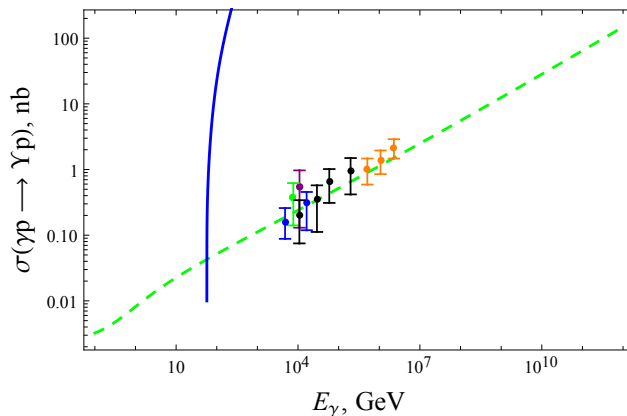


FIG. 15: Total cross section for photoproduction of upsilononium with $V = \Upsilon$ from close to threshold to the very high energy regime. The solid (blue) curve is the low-energy regime (near threshold). The green line (medium dashed) is found after fixing a normalization constant with one high energy data point but with the same 't Hooft coupling constant $\lambda = 11.243$ as J/ψ . The data points are from: [39] (green), [40] (purple), [41] (blue), [42] (orange), and [43] (black).

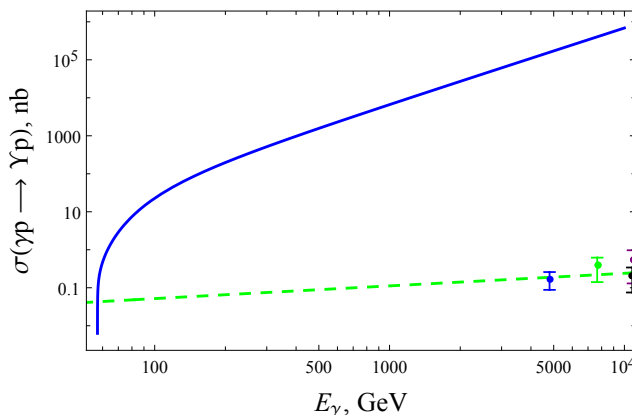


FIG. 16: Total cross section for Υ photoproduction with the same parameters as in Fig. 15 but zoomed in near the threshold.

old to very high energy. The same soft wall parameters (VIII.62) and the same fitting condition on $A(0)$ as in (VIII.63) are used in the threshold region for the solid-blue curve. In this region, the parameter set is insensitive to the expansion of the vector meson wavefunction $L_n^1(z)$ near the holographic boundary. At very high energy, we used the parameter set (VIII.62) for the D9 model and adjusted $A(0, j_0)$ to

$$\left(\frac{\tilde{\kappa}_N}{\tilde{\kappa}_V}\right)^{j_0} \times \frac{10 N_f A(0, j_0)}{\sqrt{\lambda}(10\tilde{\kappa}_V)^4} = 3.631 \text{ GeV}^{-4} \quad (\text{D9 model}) \quad (\text{IX.94})$$

with $\lambda = 11.243$. The fit value (IX.94) is sensitive to the expansion of $L_n^1(z)$ near the holographic boundary. The value of the coupling λ is not. Similar fits are found for the other two holographic models. The solid (blue) curve is the low-energy regime. The data are from GlueX [15](black). The red (tiny dashed) is the high energy regime. The green line (medium dashed) is found after fixing a normalization constant with one high en-

ergy data point but with the same high energy 't Hooft coupling constant $\lambda = 11.243$ as the red (tiny dashed) one. In Fig. 13, we zoomed in the total cross section for J/Ψ photoproduction near the threshold with the same parameters as in Fig. 14, and compared to data from GlueX [15] in this regime.

In Fig. 15, we show the total cross section for $V = \Upsilon$ photoproduction from close to threshold to very high energy regime, with the same parameter set. The solid (blue) curve is the low-energy regime. The green line (medium dashed) is found after fixing a normalization constant with one high energy data point but with the same 't Hooft coupling constant $\lambda = 11.243$ as J/ψ . In Fig. 16, we show the total cross section for Υ photoproduction zoomed in close to the threshold with the same parameters as in Fig. 15.

X. GENERALIZED PARTON DISTRIBUTION OF GLUONS INSIDE THE PROTON

The generalized parton distribution (GPD) can be viewed as the amplitude for removing a parton with momentum fraction- x and then re-inserting it, while the nucleon is receiving a momentum kick \vec{K} all the while travelling on the light cone. It is related to the form factor of the energy-momentum tensor by a sum rule as we now detail. The fact that the gluon GPD can be picked in the diffractive photoproduction of heavy mesons is not surprising. Indeed, as we noted earlier, the Witten diagram

$$A(K) = A(0) \times \Gamma(a_K + 2) \times g_5^2 \tilde{\kappa}_N^4 A(j=2, K) = A(0) \int_0^1 dx \frac{a_K(a_K + 1)}{x^{\alpha_G(t)}} \left(\frac{1-x}{1+x} \right)^\tau \quad (\text{X.95})$$

with the graviton Regge trajectory $\alpha_G(t) = 1 + t/m_0^2$ and $-t = K^2 \ll s$. Here m_0 is fixed by the 2^{++} glueball mass in (IV.25). For a spin-2 and twist-2 exchange, the $A(K)$ form factor obeys the sum rule [27] (see also Eq. 3.154 in [44], and reference therein)

$$A(K) \equiv \int_0^1 dx x^{j-1} g(x, K) \quad (\text{X.96})$$

with $xg(x, K)$ the gluon GPD, at the renormalization scale set by the nucleon mass.

The representation (X.95) suggests that $0 \leq x \leq 1$ maybe interpreted as the x -momentum fraction of the gluons in the proton probed by the graviton. At small- x , the exchange is dominated by the graviton Regge trajectory which is manifest in the integral representation

$$b_\perp^2 xg_{<}(x, b_\perp) \sim A(0) \frac{2\tilde{\kappa}_N^2 b_\perp^2}{\pi x} \left(\frac{1-x}{1+x} \right)^\tau \frac{e^{\frac{2\tilde{\kappa}_N^2 b_\perp^2}{\ln x}}}{\ln^5 \frac{1}{x}} \left(-4\tilde{\kappa}_N^4 b_\perp^4 + \ln x (-8\tilde{\kappa}_N^2 b_\perp^2 + \ln x (-2 + 2\tilde{\kappa}_N^2 b_\perp^2 + \ln x)) \right) \quad (\text{X.99})$$

(X.99) is seen to spread or diffuse (Gribov diffusion) in the transverse plane over a length scale fixed by $l_\perp \sim (2\ln(1/x))^{1/2}/\tilde{\kappa}_N$, with

$$b_\perp^2 xg_{<}(x, b_\perp) \sim A(0) \frac{8(\tilde{\kappa}_N b_\perp)^6}{\pi x} \left(\frac{1-x}{1+x} \right)^\tau \frac{e^{-\frac{2\tilde{\kappa}_N^2 b_\perp^2}{\ln \frac{1}{x}}}}{\ln^5 \frac{1}{x}} \quad (\text{X.100})$$

which is enhanced at low- x as $1/(x \ln^5 \frac{1}{x})$. The diffusion ceases to be semi-positive for $b_\perp < l_\perp$ or $K_\perp > 1/l_\perp$.

for the holographic photoproduction amplitude is related to the amplitude for the inverse deeply virtual Compton scattering amplitude through VMD.

A. Gluon GPD: $j = 2$

The tensor coupling of the glueball to the nucleon as a Dirac fermion is through its gravitational invariant form factors (V.39). For $j = 2$ the exchange is dominated by the graviton at threshold, with the contribution ($\tau = 3$ and $a_K = K^2/8\tilde{\kappa}_N^2$)

(X.95)

$$xg_{<}(x, K) \sim A(0) \frac{a_K(a_K + 1)}{x^{\alpha_G(t)}} \left(\frac{1-x}{1+x} \right)^\tau \quad (\text{X.97})$$

For zero skewness ($\xi = 0$), the momentum transfer is purely transverse and the spatial and transverse Fourier transform of (X.97) samples the distribution of an x -parton at a given transverse spatial distance in the light cone,

$$xg_{<}(x, b_\perp) = \int \frac{dK_\perp}{(2\pi)^2} e^{-iK_\perp \cdot b_\perp} xg_{<}(x, K_\perp) \quad (\text{X.98})$$

with

In Fig. 17 we show the behavior of the transverse gluon density (X.100) as probed by the graviton at small- x and small K_\perp or large b_\perp . The central hole in Fig. 17b occurs at small $b_\perp < l_\perp$ and falls outside the range of the diffusive approximation in (X.100).

To probe large- x and small b_\perp through (X.95), it is best to remove the large K -factors in the integrand through two integrations by parts **without modifying** the sum rule for $A(K)$. The result is

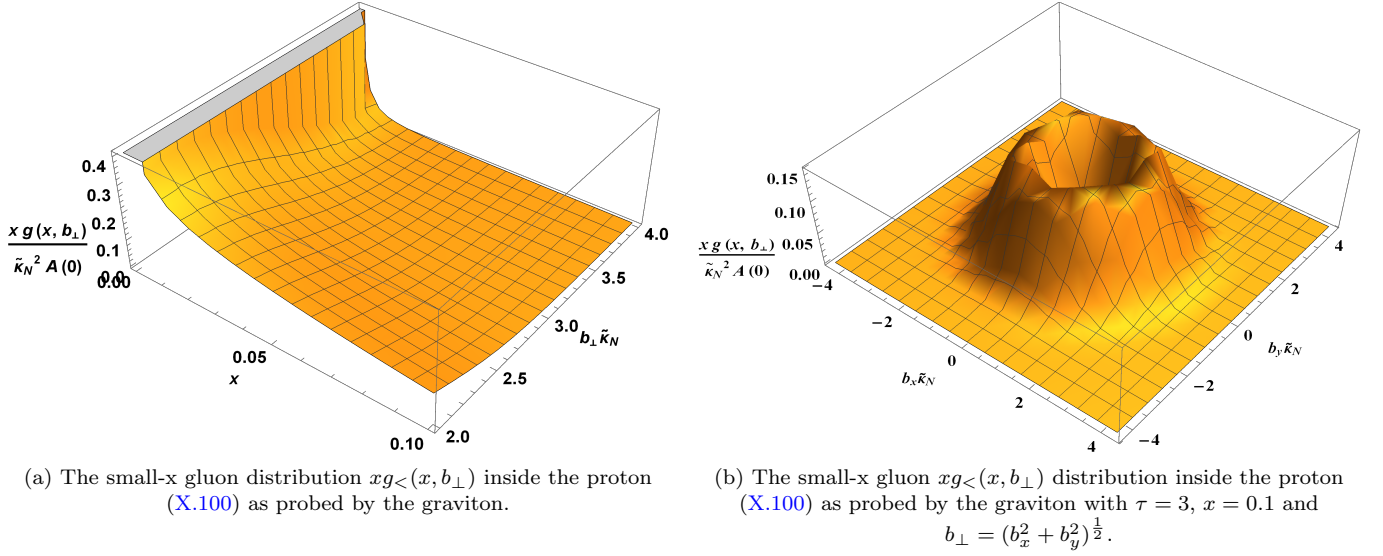


FIG. 17: Small-x gluon GPD as probed by graviton exchange in photoproduction of a heavy meson close to threshold.

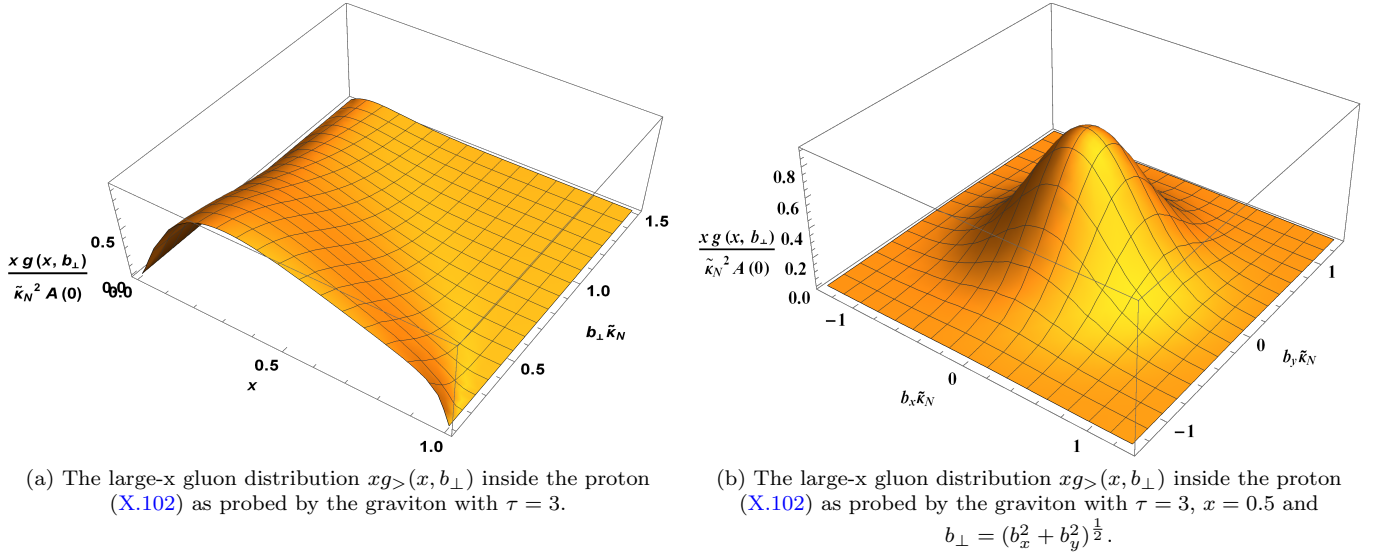


FIG. 18: Large-x gluon GPD as probed by graviton exchange in photoproduction of a heavy meson close to threshold.

$$xg_>(x, K) \sim A(0)x^{a_{\kappa}+1} \left(\left(\frac{1-x}{1+x} \right)^\tau \right)'' \quad (\text{X.101})$$

with the primes referring to x-derivatives. The corresponding transverse density at large-x is semi-positive throughout, and reads

$$b_\perp^2 xg_>(x, b_\perp) \sim A(0)x \left(\left(\frac{1-x}{1+x} \right)^\tau \right)'' \frac{2(\tilde{\kappa}b_\perp)^2}{\pi} \frac{e^{-\frac{2\tilde{\kappa}_N^2 b_\perp^2}{\ln \frac{1}{x}}}}{\ln \frac{1}{x}} \quad (\text{X.102})$$

In Fig. 18a we show the large-x behavior of the gluon

GPD (X.102) as probed by the graviton, as a function of parton-x and the rescaled transverse size $\tilde{\kappa}_N b_\perp$ for $\tau = 3$. The GPD distribution for large-x and fixed $x = 0.5$ in the transverse plane is shown in Fig. 18b. For comparison, one can look at the GPD of valence quarks in the proton extracted from holographic QCD models in [45].

B. Gluon GPD : $j = j_0$

Higher spin-j exchanges once resummed yield Pomeron exchange at higher energies. The emerging Pomeron form factor follows from (IX.76) for $j = j_0$ in the form

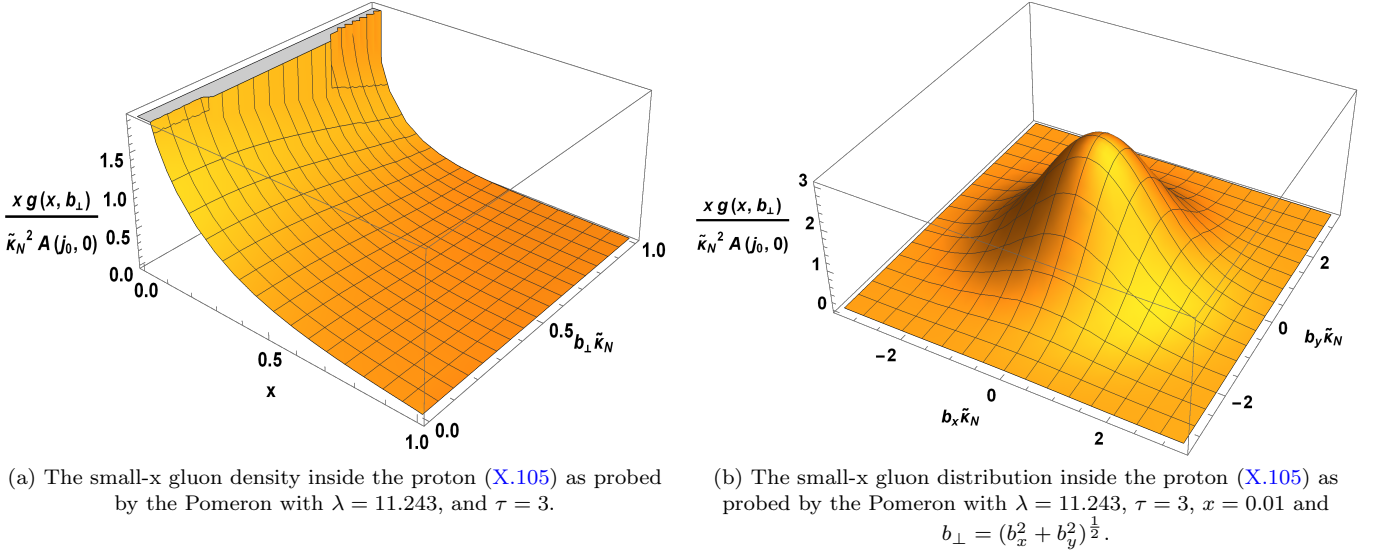


FIG. 19: Gluon GPD as probed by Pomeron exchange in photoproduction of a heavy meson at high energy.

$$\begin{aligned}
 A_P(K) &= A(j_0, 0) \Gamma(a_K + \Delta(j_0)/2) \times g_5^2 \tilde{\kappa}_N^{j_0 - 2 + \Delta(j_0)} A(j_0, K) \\
 &= A(j_0, 0) \frac{\Gamma(\tau - 1/\sqrt{\lambda})}{\Gamma(\tau)} \int_0^1 dx x^{j_0 - 1} \frac{1}{x^{\alpha_P(t)}} \left(\frac{1-x}{1+x} \right)^{\tau - \frac{1}{\sqrt{\lambda}}} \frac{1}{1-x^2} \left((\tau - 1)(1+x) + \left(\tau - \frac{1}{\sqrt{\lambda}} \right)(1-x) \right)
 \end{aligned}
 \tag{X.103}$$

with the Pomeron trajectory $\alpha_P(t) = 1 - 2/\sqrt{\lambda} + t/m_0^2$, and with m_0 fixed by the 2^{++} glueball mass in (IV.25). By analogy with the $j = 2$ exchange, we suggest that the gluon content of the proton as probed by the Pomeron for

small K is concentrated at small- x , and follows from the dominant Pomeron exchange which is manifest in (X.103) as

$$xg(x, K) \sim A(j_0, 0) \frac{\Gamma(\tau - 1/\sqrt{\lambda})}{\Gamma(\tau)} \frac{1}{x^{\alpha_P(t)}} \left(\frac{1-x}{1+x} \right)^{\tau - \frac{1}{\sqrt{\lambda}}} \frac{1}{1-x^2} \left((\tau - 1)(1+x) + \left(\tau - \frac{1}{\sqrt{\lambda}} \right)(1-x) \right)
 \tag{X.104}$$

The corresponding transverse gluon density is

$$b_{\perp}^2 xg(x, b_{\perp}) \sim A(j_0, 0) \frac{\Gamma(\tau - 1/\sqrt{\lambda})}{\Gamma(\tau)} \left(\frac{1-x}{1+x} \right)^{\tau - \frac{1}{\sqrt{\lambda}}} \frac{1}{1-x^2} \left((\tau - 1)(1+x) + \left(\tau - \frac{1}{\sqrt{\lambda}} \right)(1-x) \right) \frac{2(\tilde{\kappa} b_{\perp})^2 e^{-\frac{2\tilde{\kappa}_N^2 b_{\perp}^2}{\ln \frac{1}{x}}}}{\pi x^{1 - \frac{2}{\sqrt{\lambda}}} \ln \frac{1}{x}}
 \tag{X.105}$$

In Fig. 19a we show the behavior of the transverse gluon density probed by the Pomeron in (X.105), for $\lambda = 11.243$, $\tau = 3$. The same density is shown in Fig. 19b for fixed $x = 0.01$. We note that the low- x contribution

probed by the Pomeron at high energy or equivalently large rapidity $\chi = \ln(s/s_{\text{tr}}) \gg 1$ far from threshold, is substantially larger than the one probed by the graviton close to threshold at small rapidity $\chi = \ln(s/s_{\text{tr}}) \sim 1$.

Also, we note that at high energy, the transverse gluon density probed by the Pomeron is diffusive-like throughout.

C. Skewed Gluon GPD

The gluonic skewed GPD for the energy momentum tensor with finite skewness $\xi = K_z/2\sqrt{m_N^2 + K^2}/4$, are related to the invariant form factors in (V.39) through (see Eq. 3.127 and Eq. 3.151 in [44], and references therein)

$$\begin{aligned} \int_0^1 dx H^g(x, \xi, K) &= A(K) + \xi^2 D(K) \rightarrow (1 - 4\xi^2)A(K) \\ \int_0^1 dx E^g(x, \xi, K) &= B(K) - \xi^2 D(K) \rightarrow 4\xi^2 A(K) \end{aligned} \quad (\text{X.106})$$

with the rightmost results following from our holographic results for the invariant form factors, $B(K) = 0$ and $D(K) = 4C(K) = -4A(K)$. In terms of (X.100-X.102) (graviton) or (X.104) (Pomeron), we have for the skewed gluonic distributions

$$\begin{aligned} H^g(x, \xi, K) &= (1 - 4\xi^2) xg(x, K) \\ E^g(x, \xi, K) &= 4\xi^2 xg(x, K) \end{aligned} \quad (\text{X.107})$$

which amounts to the gluonic contribution to Ji's sum rule [46] as

$$J^{gluon}(0) = \frac{1}{2} \int_0^1 dx (H^g(x, \xi, 0) + E^g(x, \xi, 0)) = \frac{1}{2} A(0) \quad (\text{X.108})$$

As we noted in (VIII.63), the extraction of $A(0)$ from the threshold photoproduction data is model dependent.

XI. CONCLUSIONS

We have analyzed heavy meson photoproduction for all \sqrt{s} , using a bottom-up approach holographic construction. We have used the Witten diagrams in AdS₅ for diffractive photoproduction of J/ψ , shown in Fig. 2, and explicitly computed the differential cross section for the heavy meson production, first near threshold, where it is dominated by the exchange of massive 2^{++} glueballs as spin-2 gravitons in bulk, and second away from threshold, where the exchange involves a tower of spin-j states that transmute to the Pomeron. Our construction is general, and carries readily to heavier meson production such as Υ . We have presented direct predictions for this production near and away from threshold.

Our analysis allowed for the explicit derivation of all three holographic gravitational form factors $A(k), B(k), C(k)$. In the double limit of a large number of colors and strong coupling, the holographic approach is dual to quenched QCD, so the form factors are mostly gluonic. Indeed, we have found that the form factors $A(k)$ and $D(k) = 4C(k)$ compare well to the gluonic gravitational form factors from the recent lattice QCD simulations [26]. The exception is the form factor $C(k)$ where a strong mixing on the lattice with the low-lying scalar-isoscalar was noted. We have used the $D(k)$ form factor to determine the distribution of the pressure and shear inside the proton. The results are comparable to those extracted recently from the lattice [28], and empirical data in [29].

We have found that the differential cross section for the photoproduction of heavy meson production, is solely dependent on the invariant form factor $A(k)$ in our holographic analysis. The agreement of the differential and total cross sections with the recently reported GlueX data for J/Ψ production near threshold [15], suggests that the heavy meson production is controlled by the tensor 2^{++} glueball as a graviton exchange in bulk. Indeed, it is the graviton Regge trajectory at low \sqrt{s} that transmutes to the Pomeron Regge trajectory at large \sqrt{s} in holography, thereby providing a unified description of the photoproduction process of heavy mesons at all energies. These results complement those presented originally in [4, 5] away from threshold, and are overall consistent with some of the general observations presented recently in [17, 18] close to threshold.

From a pertinent integral representation of $A(k)$ in the soft-wall model, we have determined the GPD of the gluons in the proton as probed by the spin-2 glueball or graviton near threshold, and the Pomeron way above threshold in the photoproduction process. The holographic construction clearly shows that the GlueX experiment [15] directly probes the tensor gluonic contribution of the energy form factor in the nucleon state as a bulk Dirac fermion. Conversely, we have used the GlueX data in combination with our holographic cross section result to extract in an almost model independent way the gravitational form factor $A(k)$ modulo $A(0)$, and consequently the gluon GPD of the proton. The value of $A(0)$ as it relates to the gluonic contribution to the proton spin is model dependent, and cannot be reliably extracted from the threshold data in the photoproduction process. Our observations are overall consistent with the original arguments presented in [19] using short distance QCD methods.

The forthcoming high statistics measurements from SoLID [16] will provide further insights and checks on the present holographic analysis.

XII. ACKNOWLEDGEMENTS

We thank Zein-Eddine Meziani for discussions. This work was supported by the U.S. Department of Energy under Contract No. DE-FG-88ER40388.

XIII. APPENDIX: WAVEFUNCTIONS AND PROPAGATORS IN HOLOGRAPHIC QCD

A. Dirac fermion/proton

The normalized wavefunctions for the bulk Dirac fermion are [21]

$$\begin{aligned}\Psi(p, z) &= \psi_R(z)\Psi_R^0(p) + \psi_L(z)\Psi_L^0(p), \\ \bar{\Psi}(p, z) &= \bar{\psi}_R(z)\bar{\Psi}_R^0(p) + \bar{\psi}_L(z)\bar{\Psi}_L^0(p),\end{aligned}\tag{XIII.109}$$

where for the **hard-wall**

$$\begin{aligned}\psi_R(z) &= \frac{\sqrt{2}z^{5/2}J_{\tau-2}(m_N z)}{z_0 J_{\tau-1}(m_N z_0)}, \\ \psi_L(z) &= \frac{\sqrt{2}z^{5/2}J_{\tau-1}(m_N z)}{z_0 J_{\tau-1}(m_N z_0)},\end{aligned}\tag{XIII.110}$$

with the Bessel functions $J_\alpha(m_N z)$, and for the **soft-wall**

$$\begin{aligned}\psi_R(z) &= \frac{\tilde{n}_R}{\tilde{\kappa}_N^{\tau-2}} z^{\frac{5}{2}} \xi^{\frac{\tau-2}{2}} L_0^{(\tau-2)}(\xi), \\ \psi_L(z) &= \frac{\tilde{n}_L}{\tilde{\kappa}_N^{\tau-1}} z^{\frac{5}{2}} \xi^{\frac{\tau-1}{2}} L_0^{(\tau-1)}(\xi),\end{aligned}\tag{XIII.111}$$

with the generalized Laguerre polynomials $L_n^{(\alpha)}(\xi)$, $\tilde{n}_R = \tilde{n}_L \tilde{\kappa}_N^{-1} \sqrt{\tau-1}$, and $\tilde{n}_L = \tilde{\kappa}_N^\tau \sqrt{2/\Gamma(\tau)}$. The bulk wave functions are normalized for the **hard-wall** as

$$\int_0^{z_0} dz \sqrt{g} e_a^\mu \psi_{R/L}^2(z) = \delta_a^\mu,\tag{XIII.112}$$

and for the **soft-wall** as

$$\int_0^\infty dz \sqrt{g} e^{-\phi} e_a^\mu \psi_{R/L}^2(z) = \delta_a^\mu,\tag{XIII.113}$$

with $\phi = \tilde{\kappa}_N^2 z^2$, and the inverse vielbein $e_a^\mu = \sqrt{|g^{\mu\mu}|} \delta_a^\mu$ (no summation intended in μ).

For both the hard-wall and soft-wall models, we have the twist parameter $\tau = 3$, $\Psi_{R/L}^0(p) = P_\pm u(p)$, $\bar{\Psi}_{R/L}^0(p) = \bar{u}(p)P_\mp$, and $P_\pm = (1/2)(1 \pm \gamma^5)$. We also work with the normalizations of the boundary constant spinors for both the hard-wall and soft-wall models as

$$\begin{aligned}\bar{u}(p)u(p) &= 2m_N, \\ 2m_N \times \bar{u}(p')\gamma^\mu u(p) &= \bar{u}(p')(p' + p)^\mu u(p).\end{aligned}\tag{XIII.114}$$

B. Photon/spin-1 mesons

1. Hard wall

For time-like momenta ($q^2 > 0$), the non-normalizable wave function for the virtual photon is generally given by $A_\mu = V(q, z) n_\mu e^{-iq \cdot x}$ where [47, 48]

$$V(q, z) = -g_5 \sum_n \frac{F_n \phi_n(z)}{q^2 - m_n^2},\tag{XIII.115}$$

with $V(0, z) = V(q, 0) = 1$, the decay constant of the vector mesons $F_n = (1/g_5)(-\frac{1}{z'}\partial_{z'}\phi_n(z'))|_{z'=\epsilon}$, and the normalized wave functions of the vector mesons $A_\mu = \phi_n(z) n_\mu e^{-q \cdot x}$

$$\phi_n(z) = c_n z J_1(m_n z) \equiv J_A(m_n, z),\tag{XIII.116}$$

with $c_n = \frac{\sqrt{2}}{z_0 J_1(m_n z_0)}$, which satisfy the normalization condition

$$\int dz \sqrt{g} (g^{xx})^2 \phi_n(z) \phi_m(z) = \delta_{nm}.\tag{XIII.117}$$

In the hard-wall model, the summation in (XIII.115) can be carried out analytically and is given by

$$V(q, z) = \frac{\pi}{2} z q \left(\frac{Y_0(qz_0)}{J_0(qz_0)} J_1(qz) - Y_1(qz) \right).\tag{XIII.118}$$

For space-like momenta ($q^2 = -Q^2$), the non-normalizable wave function for the virtual photon is generally given by $A_\mu = \mathcal{V}(Q, z) n_\mu e^{-q \cdot x}$ where

$$\mathcal{V}(Q, z) = g_5 \sum_n \frac{F_n \phi_n(z)}{Q^2 + m_n^2}.\tag{XIII.119}$$

For example, in the hard-wall model, the summation in (XIII.119) can be carried out analytically and is given by

$$\mathcal{V}(Q, z) = Qz \left(\frac{K_0(Qz_0)}{I_0(Qz_0)} I_1(Qz) + K_1(Qz) \right),\tag{XIII.120}$$

with the normalization $\mathcal{V}(0, z) = \mathcal{V}(Q, 0) = 1$.

The bulk-to-bulk propagator for the massive mesons, for time-like momenta ($q^2 > 0$), can be written as

$$G_{\mu\nu}(z, z') = \mathcal{T}_{\mu\nu} G(z, z') = \left(-\eta_{\mu\nu} + \frac{k_\mu k_\nu}{m_n^2} \right) G(z, z'),\tag{XIII.121}$$

with

$$G(z, z') = \sum_n \frac{\phi_n(z)\phi_n(z')}{q^2 - m_n^2}. \quad (\text{XIII.122})$$

$$G(z \rightarrow 0, z') \approx \frac{\phi_n(z \rightarrow 0)}{-g_5 F_n} \sum_n \frac{-g_5 F_n \phi_n(z')}{q^2 - m_n^2} = \frac{z^2}{2} \sum_n \frac{-g_5 F_n \phi_n(z')}{q^2 - m_n^2} = \frac{z^2}{2} V(q, z'), \quad (\text{XIII.123})$$

where we used

$$F_n = (1/g_5) \left(-\frac{1}{z'} \partial_{z'} \phi_n(z') \right) \Big|_{z'=\epsilon} = -\frac{1}{g_5} c_n m_n, \quad (\text{XIII.124})$$

and $\phi_n(z \rightarrow 0) \approx \frac{1}{2} c_n m_n z^2$ for the hard-wall. Defining the decay constant as $f_n = -\frac{F_n}{m_n}$, we have

$$\phi_n(z) = \frac{f_n}{m_n} \times g_5 m_n z J_1(m_n z), \quad (\text{XIII.125})$$

as required by vector meson dominance (VMD). For space-like momenta ($q^2 = -Q^2$), we have

$$G(z \rightarrow 0, z') \approx \frac{z^2}{2} \sum_n \frac{g_5 F_n \phi_n(z')}{Q^2 + m_n^2} = \frac{z^2}{2} \mathcal{V}(Q, z'). \quad (\text{XIII.126})$$

2. Soft wall

Similar relationships hold for the soft-wall model where the normalized wave function for vector mesons is given by [49]

$$\phi_n(z) = c_n \tilde{\kappa}_V^2 z^2 L_n^1(\tilde{\kappa}_V^2 z^2) \equiv J_A(m_n, z), \quad (\text{XIII.127})$$

$$G(z \rightarrow 0, z') \approx \frac{\phi_n(z \rightarrow 0)}{-g_5 F_n} \sum_n \frac{-g_5 F_n \phi_n(z')}{q^2 - m_n^2} = \frac{z^2}{2} \sum_n \frac{-g_5 F_n \phi_n(z')}{q^2 - m_n^2} = \frac{z^2}{2} V(q, z'). \quad (\text{XIII.131})$$

For space-like momenta ($q^2 = -Q^2$), we have the bulk-to-bulk propagator near the boundary

For space-like momenta $q^2 = -Q^2$ in (XIII.122). Also recall that $\mathcal{V}(q, z) = \frac{1}{z'} \partial_{z'} G(z, z') \Big|_{z'=\epsilon}$. Note that for $z \rightarrow 0$, we can write (XIII.122) as

with $c_n = \sqrt{2/n+1}$ which is determined from the normalization condition (for the soft-wall model with background dilaton $\phi = \tilde{\kappa}_V^2 z^2$)

$$\int dz \sqrt{g} e^{-\phi} (g^{xx})^2 \phi_n(z) \phi_m(z) = \delta_{nm}. \quad (\text{XIII.128})$$

Therefore, we have

$$F_n = \frac{1}{g_5} \left(-e^{-\phi} \frac{1}{z'} \partial_{z'} \phi_n(z') \right) \Big|_{z'=\epsilon} = -\frac{2}{g_5} c_n (n+1) \tilde{\kappa}_V^2, \quad (\text{XIII.129})$$

with $\phi_n(z \rightarrow 0) \approx c_n \tilde{\kappa}_V^2 z^2 (n+1)$. If we define the decay constant as $f_n = -F_n/m_n$, we have

$$\phi_n(z) = \frac{f_n}{m_n} \times 2g_5 \tilde{\kappa}_V^2 z^2 L_n^1(\tilde{\kappa}_V^2 z^2), \quad (\text{XIII.130})$$

as required by vector meson dominance (VMD).

Note that for $z \rightarrow 0$, we can write the bulk-to-bulk propagator (XIII.122) as

$$G(z \rightarrow 0, z') \approx \frac{z^2}{2} \sum_n \frac{g_5 F_n \phi_n(z')}{Q^2 + m_n^2} = \frac{z^2}{2} \mathcal{V}(Q, z'), \quad (\text{XIII.132})$$

where [49]

$$\mathcal{V}(Q, z) = \kappa_V^2 z^2 \int_0^1 \frac{dx}{(1-x)^2} x^a \exp\left[-\frac{x}{1-x} \kappa_V^2 z^2\right], \quad (\text{XIII.133})$$

with the normalization $\mathcal{V}(0, z) = \mathcal{V}(Q, 0) = 1$.

C. Transverse-traceless graviton/spin-2 glueballs

1. Hard wall

For time-like momenta ($k^2 > 0$), the non-normalizable wave function for the virtual transverse-traceless graviton is generally given by $h_{\mu\nu} = h(k, z) \epsilon_{\mu\nu}^{TT} e^{-ik \cdot x}$ where [50]

$$h(k, z) = -\sqrt{2}\kappa \sum_n \frac{F_n \psi_n(z)}{k^2 - m_n^2}, \quad (\text{XIII.134})$$

with the normalization $h(0, z) = h(k, 0) = 1$, which could be relaxed. The decay constant of the spin-2 glueball with mass m_n is

$$F_n = \frac{1}{\sqrt{2}\kappa_V} \left(-\frac{1}{z'^3} \partial_{z'} \psi_n(z') \right)_{z'=\epsilon} \quad (\text{XIII.135})$$

and the normalized wave functions of the spin-2 glueballs $h_{\mu\nu} = \psi_n(z) \epsilon_{\mu\nu}^{TT} e^{-ik \cdot x}$

$$\psi_n(z) = c_n z^2 J_2(m_n z) \equiv J_h(m_n, z), \quad (\text{XIII.136})$$

with $c_n = \frac{\sqrt{2}}{z_0 J_2(m_n z_0)}$, which satisfy the normalization condition

$$\int dz \sqrt{g} |g^{xx}| \psi_n(z) \psi_m(z) = \delta_{nm}. \quad (\text{XIII.137})$$

In the hard-wall model, the summation in (XIII.134) can be carried out analytically and is given by [21, 48, 50]

$$h(k, z) = \frac{\pi}{4} k^2 z^2 \left(\frac{Y_1(kz_0)}{J_1(kz_0)} J_2(kz) - Y_2(kz) \right). \quad (\text{XIII.138})$$

For space-like momenta ($k^2 = -K^2$), the non-normalizable wave function for the virtual transverse-traceless graviton is generally given by $h_{\mu\nu} = \mathcal{H}(K, z) \epsilon_{\mu\nu}^{TT} e^{-ik \cdot x}$ where

$$\mathcal{H}(K, z) = \sqrt{2}\kappa \sum_n \frac{F_n \psi_n(z)}{K^2 + m_n^2}. \quad (\text{XIII.139})$$

In the hard-wall model, the summation in (XIII.139) can be carried out analytically and is given by [21, 48, 50]

$$\mathcal{H}(K, z) = \frac{1}{2} K^2 z^2 \left(\frac{K_1(Kz_0)}{I_1(Kz_0)} I_2(Kz) + K_2(Kz) \right). \quad (\text{XIII.140})$$

For time-like momenta ($q^2 > 0$), the bulk-to-bulk propagator for the massive spin-2 glueballs, can be written as [21, 48, 50]

$$G_{\mu\nu\alpha\beta}^{TT}(z, z') = \frac{1}{2} \left(\mathcal{T}_{\mu\alpha} \mathcal{T}_{\nu\beta} + \mathcal{T}_{\mu\beta} \mathcal{T}_{\nu\alpha} - \frac{2}{3} \mathcal{T}_{\mu\nu} \mathcal{T}_{\alpha\beta} \right) G(z, z'), \quad (\text{XIII.141})$$

with $\mathcal{T}_{\mu\nu} = -\eta_{\mu\nu} + k_\mu k_\nu / m_n^2$ and

$$G(z, z') = \sum_n \frac{\psi_n(z) \psi_n(z')}{k^2 - m_n^2}. \quad (\text{XIII.142})$$

For space-like momenta, we simply replace $k^2 = -K^2$ in (XIII.142). Also remember that

$$h(k, z) = \frac{1}{z'^3} \partial_{z'} G(z, z')|_{z'=\epsilon}. \quad (\text{XIII.143})$$

Note that for $z \rightarrow 0$, we can write (XIII.142) as

$$G(z \rightarrow 0, z') \approx \frac{z^4}{4} \sum_n \frac{-\sqrt{2}\kappa F_n \psi_n(z')}{k^2 - m_n^2} = \frac{z^4}{4} h(k, z'), \quad (\text{XIII.144})$$

where we used

$$F_n = \frac{1}{\sqrt{2}\kappa} \left(-\frac{1}{z'^3} \partial_{z'} \psi_n(z') \right)_{z'=\epsilon} = -\frac{1}{2\sqrt{2}\kappa} c_n m_n^2, \quad (\text{XIII.145})$$

and $\psi_n(z \rightarrow 0) \approx \frac{1}{8} c_n m_n^2 z^4$ for the hard-wall. Hence, for space-like momenta ($k^2 = -K^2$), we have

$$G(z \rightarrow 0, z') \approx \frac{z^4}{4} \sum_n \frac{\sqrt{2}\kappa_V F_n \phi_n(z')}{K^2 + m_n^2} = \frac{z^4}{4} \mathcal{H}(K, z'). \quad (\text{XIII.146})$$

2. Soft wall

Similar relationships hold for the soft-wall model where the normalized wave function for spin-2 glueballs is given by [51] (note that the discussion in [51] is for general

massive bulk scalar fluctuation but can be used for spin-2 glueball which has an effective bulk action similar to massless bulk scalar fluctuation)

$$\psi_n(z) = c_n z^4 L_n^{\Delta(j)-2}(2\xi), \quad (\text{XIII.147})$$

with

$$c_n = \left(\frac{2^4 \tilde{\kappa}_N^6 \Gamma(n+1)}{\Gamma(n+3)} \right)^{\frac{1}{2}}, \quad (\text{XIII.148})$$

which is determined from the normalization condition (for soft-wall model with background dilaton $\phi = \tilde{\kappa}_N^2 z^2$)

$$\int dz \sqrt{g} e^{-\phi} |g^{xx}| \psi_n(z) \psi_m(z) = \delta_{nm}. \quad (\text{XIII.149})$$

Therefore we have

$$F_n = \frac{1}{\sqrt{2\kappa}} \left(-\frac{1}{z'^3} \partial_{z'} \psi_n(z') \right)_{z'=\epsilon} = -\frac{4}{\sqrt{2\kappa}} c_n L_n^2(0), \quad (\text{XIII.150})$$

with $\psi_n(z \rightarrow 0) \approx c_n z^4 L_n^2(0)$. For space-like momenta ($q^2 = -Q^2$), we have the bulk-to-bulk propagator near the boundary

$$G(z \rightarrow 0, z') \approx \frac{z^4}{4} \sum_n \frac{\sqrt{2\kappa} F_n \phi_n(z')}{K^2 + m_n^2} = \frac{z^4}{4} \mathcal{H}(K, z'), \quad (\text{XIII.151})$$

where, for the soft-wall model, [21, 48, 51]

$$\begin{aligned} \mathcal{H}(K, z) &= 4z^4 \Gamma(a_K + 2) U(a_K + 2, 3; 2\xi) = \Gamma(a_K + 2) U(a_K, -1; 2\xi) \\ &= \frac{\Gamma(a_K + 2)}{\Gamma(a_K)} \int_0^1 dx x^{a_K - 1} (1-x) \exp\left(-\frac{x}{1-x} (2\xi)\right), \end{aligned} \quad (\text{XIII.152})$$

with $a_K = a/2 = K^2/8\tilde{\kappa}_N^2$, and we have used the transformation $U(m, n; y) = y^{1-n} U(1+m-n, 2-n, y)$. (XIII.152) satisfies the normalization condition $\mathcal{H}(0, z) = \mathcal{H}(K, 0) = 1$.

D. Trace-full graviton/spin-0 glueballs

1. Hard wall

For time-like momenta ($k^2 > 0$), the non-normalizable wave function for the virtual trace-full graviton is generally given by $h_{\mu\nu} = k^2 f(k, z) \epsilon_{\mu\nu}^T e^{-ik \cdot x}$ where

$$f(k, z) = 2\sqrt{2\kappa} \sum_n \frac{F_n \psi_n(z)}{k^2 - m_n^2}, \quad (\text{XIII.153})$$

with $f(0, z) = f(k, 0) = 1$, the decay constant of the spin-0 glueballs $F_n = \frac{1}{2\sqrt{2\kappa}} \left(\frac{1}{z'^3} \partial_{z'} \psi_n(z') \right)_{z'=\epsilon}$, and the normalized wave functions of the spin-0 glueballs $h_{\mu\nu} = \psi_n(z) \epsilon_{\mu\nu}^T e^{-k \cdot x}$ which satisfy the normalization condition

$$\int dz \sqrt{g} |g^{xx}| \psi_n(z) \psi_m(z) = \delta_{nm}, \quad (\text{XIII.154})$$

with the normalized wave functions for the spin-0 glueballs

$$\psi_n(z) = c_n z^2 J_2(m_n z) \equiv J_f(m_n, z), \quad (\text{XIII.155})$$

where $c_n = \frac{\sqrt{2}}{z_0 J_2(m_n z_0)}$. In the hard-wall model, the summation in (XIII.153) can be carried out analytically and is given by

$$f(k, z) = \frac{\pi}{4} k^2 z^2 \left(\frac{Y_1(kz_0)}{J_1(kz_0)} J_2(kz) - Y_2(kz) \right). \quad (\text{XIII.156})$$

For space-like momenta ($k^2 = -K^2$), the non-normalizable wave function for the virtual trace-full graviton is generally given by $h_{\mu\nu} = \mathcal{F}(K, z) \epsilon_{\mu\nu}^T e^{-k \cdot x}$ where

$$\mathcal{F}(K, z) = -2\sqrt{2\kappa} \sum_n \frac{F_n \psi_n(z)}{K^2 + m_n^2}. \quad (\text{XIII.157})$$

The summation in (XIII.157) can be carried out analytically and is given by

$$\mathcal{F}(K, z) = \frac{1}{2} K^2 z^2 \left(\frac{K_1(Kz_0)}{I_1(Kz_0)} I_2(Kz) + K_2(Kz) \right). \quad (\text{XIII.158})$$

For time-like momenta ($q^2 > 0$), the bulk-to-bulk propagator for the massive spin-0 glueballs, can be written as

$G_{\mu\nu\alpha\beta}^T(z, z') = \eta_{\mu\nu}\eta_{\alpha\beta}G(z, z')$ where

$$G(z, z') = \sum_n \frac{\psi_n(z)\psi_n(z')}{k^2 - m_n^2}. \quad (\text{XIII.159})$$

with

$$f(k, z) = \left(\frac{1}{z'^3} \partial_{z'} G(z, z') \right)_{z'=\epsilon}. \quad (\text{XIII.160})$$

Note that for $z \rightarrow 0$, we can write (XIII.159) as

$$G(z \rightarrow 0, z') \approx \frac{z^4}{4} \sum_n \frac{2\sqrt{2}\kappa F_n \psi_n(z')}{k^2 - m_n^2} = \frac{z^4}{4} f(k, z'), \quad (\text{XIII.161})$$

where we used

$$F_n = \frac{1}{2\sqrt{2}\kappa} \left(\frac{1}{z'^3} \partial_{z'} G(z, z') \right)_{z'=\epsilon} = \frac{1}{4\sqrt{2}\kappa} c_n m_n^2, \quad (\text{XIII.162})$$

and $\psi_n(z \rightarrow 0) \approx \frac{1}{8} c_n m_n^2 z^4$ for the hard-wall. Hence, for space-like momenta ($k^2 = -K^2$), we have

$$G(z \rightarrow 0, z') \approx \frac{z^4}{4} \sum_n \frac{-2\sqrt{2}\kappa F_n \phi_n(z')}{K^2 + m_n^2} = \frac{z^4}{4} \mathcal{F}(K, z'). \quad (\text{XIII.163})$$

2. Soft wall

Note that similar relationships hold for the trace-full graviton/spin-0 glueball in the soft-wall model. We do not detail them here as they are similar to the ones given for the spin-2 glueballs modilo normalization constants.

E. Dilaton/spin-0 glueballs

1. Hard wall

For time-like momenta ($k^2 > 0$), the non-normalizable wave function for the virtual dilaton is generally given by

$$\varphi(k, z) = \sqrt{2}\kappa \sum_n \frac{F_n \psi_n(z)}{k^2 - m_n^2}, \quad (\text{XIII.164})$$

with $\varphi(0, z) = \varphi(k, 0) = 1$, the decay constant of the spin-0 glueballs $F_n = \frac{1}{\sqrt{2}\kappa} \left(\frac{1}{z'^3} \partial_{z'} \psi_n(z') \right)_{z'=\epsilon}$, and the normalized wave functions of the spin-0 glueballs $\psi_n(z)$ which satisfy the normalization condition

$$\int dz \sqrt{g} |g^{xx}| \psi_n(z) \psi_m(z) = \delta_{nm}, \quad (\text{XIII.165})$$

with the normalized wave functions for the spin-0 glueballs

$$\psi_n(z) = c_n z^2 J_2(m_n z) \equiv J_\varphi(m_n, z), \quad (\text{XIII.166})$$

where $c_n = \frac{\sqrt{2}}{z_0 J_2(m_n z_0)}$. For example, in the hard-wall model, the summation in (XIII.164) can be carried out analytically and is given by

$$\varphi(k, z) = \frac{\pi}{4} k^2 z^2 \left(\frac{Y_1(kz_0)}{J_1(kz_0)} J_2(kz) - Y_2(kz) \right). \quad (\text{XIII.167})$$

For space-like momenta ($k^2 = -K^2$), the non-normalizable wave function for the virtual dilaton is generally given by

$$\mathcal{D}(K, z) = -\sqrt{2}\kappa \sum_n \frac{F_n \psi_n(z)}{K^2 + m_n^2}. \quad (\text{XIII.168})$$

For example, in the hard-wall model, the summation in (XIII.168) can be carried out analytically and is given by

$$\mathcal{D}(K, z) = \frac{1}{2} K^2 z^2 \left(\frac{K_1(Kz_0)}{I_1(Kz_0)} I_2(Kz) + K_2(Kz) \right). \quad (\text{XIII.169})$$

For time-like momenta ($q^2 > 0$), the bulk-to-bulk propagator for the massive spin-0 glueballs, can be written as

$$G(z, z') = \sum_n \frac{\psi_n(z)\psi_n(z')}{k^2 - m_n^2}. \quad (\text{XIII.170})$$

We recall that $\varphi(q, z) = \frac{1}{z'^3} \partial_{z'} G(z, z')|_{z'=\epsilon}$.

Note that for $z \rightarrow 0$, we can write (XIII.170) as

$$G(z \rightarrow 0, z') \approx \frac{z^4}{4} \sum_n \frac{\sqrt{2}\kappa F_n \psi_n(z')}{k^2 - m_n^2} = \frac{z^4}{4} \varphi(k, z'), \quad (\text{XIII.171})$$

where we used

$$F_n = \frac{1}{2\sqrt{2}\kappa} \left(\frac{1}{z'^3} \partial_{z'} G(z, z') \right)_{z'=\epsilon} = \frac{1}{4\sqrt{2}\kappa} c_n m_n^2, \quad (\text{XIII.172})$$

and $\psi_n(z \rightarrow 0) \approx \frac{1}{8} c_n m_n^2 z^4$ for the hard-wall. Hence, for space-like momenta ($k^2 = -K^2$), we have

$$G(z \rightarrow 0, z') \approx \frac{z^4}{4} \sum_n \frac{-2\sqrt{2}\kappa F_n \phi_n(z')}{K^2 + m_n^2} = \frac{z^4}{4} \mathcal{D}(K, z'). \quad (\text{XIII.173})$$

2. Soft wall

Note again, that similar relationships hold for the dilaton/spin-0 glueballs in the soft-wall model, but we do not go into details here as it is very similar to the spin-2 glueballs upto normalization constants.

XIV. APPENDIX: CONTRIBUTIONS TO HOLOGRAPHIC PHOTOPRODUCTION

Here most of the results will be given for the soft wall model explicitly. The results for the hard wall model follow by setting $\phi = 0$.

A. Dilaton contribution

The dilaton contribution to the holographic photoproduction amplitude can be determined from Fig. 2 by re-

$$\begin{aligned}
 i\mathcal{A}_{Ap \rightarrow Ap}^\varphi(s, t) &= \sum_n i\tilde{\mathcal{A}}_{Ap \rightarrow Ap}^\varphi(m_n, s, t) \\
 i\tilde{\mathcal{A}}_{Ap \rightarrow Ap}^\varphi(m_n, s, t) &= (-i)V_{\varphi AA}(q_1, q_2, k, m_n) \times \tilde{G}_\varphi(m_n, t) \times (-i)V_{\varphi \bar{\Psi} \Psi}(p_1, p_2, k, m_n),
 \end{aligned}
 \tag{XIV.174}$$

with the bulk vertices ($k = p_2 - p_1 = q_1 - q_2$)

$$\begin{aligned}
 V_{\varphi AA}(q, q', k, m_n) &\equiv \left(\frac{\delta S_{\varphi AA}^k}{\delta \varphi(k, z)} \right) J_\varphi(m_n, z) = \sqrt{2\kappa^2} \times \frac{1}{4} \int dz \sqrt{g} e^{-\phi} z^4 K(q, q', n, n', z) J_\varphi(m_n, z), \\
 V_{\varphi \bar{\Psi} \Psi}(p_1, p_2, k, m_n) &\equiv \left(\frac{\delta S_{\varphi \bar{\Psi} \Psi}^k}{\delta (\partial_z \varphi(k, z))} \right) \partial_z J_\varphi(m_n, z) + \left(\frac{\delta S_{\varphi \bar{\Psi} \Psi}^k}{\delta (\varphi(k, z))} \right) J_\varphi(m_n, z) \\
 &= \frac{\sqrt{2\kappa^2}}{2} \int dz \sqrt{g} e^{-\phi} z \bar{\Psi}(p_2, z) \left(\gamma^5 \partial_z J_\varphi(m_n, z) + k_\alpha \gamma^\alpha J_\varphi(m_n, z) \right) \Psi(p_1, z),
 \end{aligned}
 \tag{XIV.175}$$

and the bulk-to-bulk propagator

$$\begin{aligned}
 G_\varphi(m_n, t, z, z') &= J_\varphi(m_n, z) \tilde{G}_\varphi(m_n, t) J_\varphi(m_n, z'), \\
 \tilde{G}_\varphi(m_n, t) &= \frac{i}{t - m_n^2 + i\epsilon},
 \end{aligned}
 \tag{XIV.176}$$

For $z' \rightarrow 0$, and $t = -K^2$ in (XIV.176), we can use (XIII.173), which simplifies (XIV.174) as

$$\begin{aligned}
 i\mathcal{A}_{Ap \rightarrow Ap}^\varphi(s, t) &\approx (-i)\mathcal{V}_{\varphi AA}(q_1, q_2, k) \times (i) \times (-i)\mathcal{V}_{\varphi \bar{\Psi} \Psi}(p_1, p_2, k), \\
 \mathcal{V}_{\varphi AA}(q_1, q_2, k) &= \sqrt{2\kappa^2} \times \sqrt{\frac{1}{4}} \int dz \sqrt{g} e^{-\phi} z^4 K(q, q', n, n', z) \frac{z^4}{4} \\
 \mathcal{V}_{\varphi \bar{\Psi} \Psi}(p_1, p_2, k) &= \sqrt{2\kappa^2} \times \frac{1}{2} \int dz e^{-\phi} \sqrt{g} z \bar{\Psi}(p_2, z) \left(\gamma^5 \partial_z \mathcal{D}(K, z) + k_\alpha \gamma^\alpha \mathcal{D}(K, z) \right) \Psi(p_1, z).
 \end{aligned}
 \tag{XIV.177}$$

B. Graviton contribution

The graviton contribution in Fig. 2 in the diffractive part of the holographic photoproduction amplitude was

placing the spin-2 glueball propagator by spin-0 glueball propagator of dilaton as

analyzed in [52] for the Pomeron kinematics in the hard

wall model. Here we will give the results for all kinematics for both the CFT case in AdS, and the conformally broken case in walled AdS.

In AdS space, for tansverse-traceless part, Witten's diagrammatic rules give formally

$$\begin{aligned}
i\mathcal{A}_{Ap \rightarrow Ap}^h(s, t) &= \sum_n i\tilde{\mathcal{A}}_{Ap \rightarrow Ap}^h(m_n, s, t) \\
i\tilde{\mathcal{A}}_{A \rightarrow Ap}^h(m_n, s, t) &= (-i)V_{hAA}^{\mu\nu(TT)}(q, q', k, m_n) \times \tilde{G}_{\mu\nu\alpha\beta}^{TT}(m_n, t) \times (-i)V_{h\bar{\Psi}\Psi}^{\alpha\beta(TT)}(p_1, p_2, k, m_n), \\
i\mathcal{A}_{Ap \rightarrow Ap}^f(s, t) &= \sum_n i\tilde{\mathcal{A}}_{Ap \rightarrow Ap}^f(m_n, s, t) \\
i\tilde{\mathcal{A}}_{Ap \rightarrow Ap}^f(m_n, s, t) &= (-i)V_{fAA}^{\mu\nu(T)}(q, q', k, m_n) \times \tilde{G}_{\mu\nu\alpha\beta}^T(m_n, t) \times (-i)V_{f\bar{\Psi}\Psi}^{\alpha\beta(T)}(p_1, p_2, k, m_n),
\end{aligned} \tag{XIV.178}$$

with the bulk vertices ($k = p_2 - p_1 = q - q'$)

$$\begin{aligned}
V_{hAA}^{\mu\nu(TT)}(q, q', k, m_n) &\equiv \left(\frac{\delta S_{hAA}^k}{\delta(\epsilon_{\mu\nu}^{TT} h(k, z))} \right) J_h(m_n, z) = \sqrt{2\kappa^2} \times \frac{1}{2} \int dz \sqrt{g} e^{-\phi} z^4 K^{\mu\nu}(q, q', n, n', z) J_h(m_n, z), \\
V_{h\bar{\Psi}\Psi}^{\alpha\beta(TT)}(p_1, p_2, k, m_n) &\equiv \left(\frac{\delta S_{h\bar{\Psi}\Psi}^k}{\delta(\epsilon_{\alpha\beta}^{TT} h(k, z))} \right) J_h(m_n, z) = -\sqrt{2\kappa^2} \times \frac{1}{2} \int dz \sqrt{g} e^{-\phi} z \bar{\Psi}(p_2, z) \gamma^\alpha p^\beta \Psi(p_1, z) J_h(m_n, z), \\
V_{fAA}^{\mu\nu(T)}(q, q', k, m_n) &\equiv \left(\frac{\delta S_{fAA}^k}{\delta(\epsilon_{\mu\nu}^T f(k, z))} \right) J_f(m_n, z) = \\
&\sqrt{2\kappa^2} \times \frac{1}{4} \int dz \sqrt{g} e^{-\phi} z^4 \tilde{k}^2 \left(K^{\mu\nu}(q, q', n, n', z) - \frac{1}{4} \eta^{\mu\nu} K(q, q', n, n', z) \right) J_f(m_n, z), \\
V_{f\bar{\Psi}\Psi}^{\alpha\beta(T)}(p_1, p_2, k, m_n) &\equiv \left(\frac{\delta S_{f\bar{\Psi}\Psi}^k}{\delta \partial_z (\epsilon_{\alpha\beta}^T f(k, z))} \right) \partial_z J_f(m_n, z) + \left(\frac{\delta S_{f\bar{\Psi}\Psi}^k}{\delta(\epsilon_{\alpha\beta}^T f(k, z))} \right) J_f(m_n, z) = \\
&-\sqrt{2\kappa^2} \times \frac{1}{2} \int dz \sqrt{g} e^{-\phi} z \tilde{k}^2 \bar{\Psi}(p_2, z) \left(\eta^{\alpha\beta} \gamma^5 \partial_z J_f(m_n, z) + \gamma^\alpha p^\beta J_f(m_n, z) + \eta^{\alpha\beta} k_\mu \gamma^\mu J_f(m_n, z) \right) \Psi(p_1, z),
\end{aligned} \tag{XIV.179}$$

with $p = (p_1 + p_2)/2$. The bulk-to-bulk graviton propagator is $G_{\mu\nu\alpha\beta} = G_{\mu\nu\alpha\beta}^{TT} + G_{\mu\nu\alpha\beta}^T$. The transverse and

traceless TT-part describes massive 2^{++} glueballs [53, 54]

$$\begin{aligned}
G_{\mu\nu\alpha\beta}^{TT}(m_n, t, z, z') &= J_h(m_n, z) \tilde{G}_{\mu\nu\alpha\beta}^{TT}(m_n, t) J_h(m_n, z'), \\
\tilde{G}_{\mu\nu\alpha\beta}^{TT}(m_n, t) &= \frac{1}{2} \left(\mathcal{T}_{\mu\alpha} \mathcal{T}_{\nu\beta} + \mathcal{T}_{\mu\beta} \mathcal{T}_{\nu\alpha} - \frac{2}{3} \mathcal{T}_{\mu\nu} \mathcal{T}_{\alpha\beta} \right) \frac{i}{t - m_n^2 + i\epsilon},
\end{aligned}$$

with \tilde{G} the boundary propagator,

$$\mathcal{T}_{\mu\nu} = -\eta_{\mu\nu} + k_\mu k_\nu / m_n^2 \tag{XIV.180}$$

The trace-full T-part $G_{\mu\nu\alpha\beta}^T$ describes massive 0^{++} glueballs [54]

$$G_{\mu\nu\alpha\beta}^T(m_n, t, z, z') = J_f(m_n, z) \tilde{G}_{\mu\nu\alpha\beta}^T(m_n, t) J_f(m_n, z'), \quad (\text{XIV.181})$$

with the boundary propagator

$$\tilde{G}_{\mu\nu\alpha\beta}^T(m_n, t) = \eta_{\mu\nu}\eta_{\alpha\beta} \frac{i}{t - m_n^2 + i\epsilon}.$$

For $z' \rightarrow 0$, and $t = -K^2$, and $t = -K^2$ in (XIV.180) and (XIV.181). We can use (XIII.146) and (XIII.163), and simplify (XIV.178) as

$$\begin{aligned} i\mathcal{A}_{Ap \rightarrow Ap}^h(s, t) &\approx (-i)\mathcal{V}_{hAA}^{\mu\nu(TT)}(q_1, q_2, k_z) \times \left(\frac{i}{2}\eta_{\mu\alpha}\eta_{\nu\beta}\right) \times (-i)\mathcal{V}_{h\bar{\Psi}\Psi}^{\alpha\beta(TT)}(p_1, p_2, k_z), \\ i\mathcal{A}_{Ap \rightarrow Ap}^f(s, t) &\approx (-i)\mathcal{V}_{hAA}^{\mu\nu(T)}(q_1, q_2, k) \times (i\eta_{\mu\nu}\eta_{\alpha\beta}) \times (-i)\mathcal{V}_{f\bar{\Psi}\Psi}^{\alpha\beta(T)}(p_1, p_2, k), \end{aligned} \quad (\text{XIV.182})$$

with

$$\begin{aligned} \mathcal{V}_{hAA}^{\mu\nu(TT)}(q_1, q_2, k_z) &= \sqrt{2\kappa^2} \times \frac{1}{2} \int dz \sqrt{g} e^{-\phi} z^4 K^{\mu\nu}(q, q', n, n', z) \frac{z^4}{4}, \\ \mathcal{V}_{h\bar{\Psi}\Psi}^{\alpha\beta(TT)}(p_1, p_2, k_z) &= -\sqrt{2\kappa^2} \times \frac{1}{2} \int dz \sqrt{g} e^{-\phi} z \bar{\Psi}(p_2, z) \gamma^\mu p^\nu \Psi(p_1, z) \mathcal{H}(K, z), \\ \mathcal{V}_{fAA}^{\mu\nu(T)}(q_1, q_2, k) &= \sqrt{2\kappa^2} \times \frac{1}{4} \int dz \sqrt{g} e^{-\phi} z^4 \tilde{k}^2 \left(K^{\mu\nu}(q, q', n, n', z) - \frac{1}{4}\eta^{\mu\nu} K(q, q', n, n', z) \right) \frac{z^4}{4}, \\ \mathcal{V}_{f\bar{\Psi}\Psi}^{\alpha\beta(T)}(p_1, p_2, k) &= -\sqrt{2\kappa^2} \times \frac{1}{2} \times \frac{1}{2} \int dz \sqrt{g} e^{-\phi} z \tilde{k}^2 \bar{\Psi}(p_2, z) \left(\eta^{\alpha\beta} \gamma^5 \partial_z \mathcal{F}(K, z) + \gamma^\alpha p^\beta \mathcal{F}(K, z) \right. \\ &\quad \left. + \eta^{\alpha\beta} k_\mu \gamma^\mu \mathcal{F}(K, z) \right) \Psi(p_1, z). \end{aligned} \quad (\text{XIV.183})$$

XV. APPENDIX: ELEMENTS OF THE REGGEIZATION

1. Hard wall

The reggeization of the graviton exchange is obtained through the substitution [55]

$$J_h(m_n(j), z) \rightarrow \tilde{\psi}_n(j, z) = z^{-(j-2)} \psi_n(j, z) \quad (\text{XV.184})$$

followed by the summation over all spin- j exchanges using the Sommerfeld-Watson formula

$$\frac{1}{2} \sum_{j \geq 2} (s^j + (-s)^j) \rightarrow -\frac{\pi}{2} \int_{\mathbb{C}} \frac{dj}{2\pi i} \left(\frac{s^{j-2} + (-s)^{j-2}}{\sin \pi j} \right) \quad (\text{XV.185})$$

for a pertinent choice of the contour \mathbb{C} . This requires the analytical continuation of the exchanged amplitudes to the complex j -plane. For the hard-wall model, the normalized wave function is given by

$$\begin{aligned} \psi_n(j, z) &= c_n(j) z^2 J_{\tilde{\Delta}(j)}(m_n(j)z) \\ c_n(j) &= \frac{1}{\sqrt{2}z_0 J_{\tilde{\Delta}(j)}(m_n(j)z_0)} \end{aligned} \quad (\text{XV.186})$$

for $\partial_z \psi_n(j, z_0) = 0$ and

$$\begin{aligned} \tilde{\Delta}(j) &\equiv \Delta(j) - 2 \\ &= \left(4 + 2\sqrt{\lambda}(j-2) \right)^{\frac{1}{2}} = \sqrt{2\sqrt{\lambda}(j-j_0)} \end{aligned} \quad (\text{XV.187})$$

with $j_0 = 2 - \frac{2}{\sqrt{\lambda}}$ and $j \geq 2$.

For time-like momenta $k^2 > 0$: we can also determine the non-normalizable wave function for the virtual transverse-traceless spin- j glueball, as

$$h(j, k, z) = -\sqrt{2}\kappa \sum_n \frac{F_n(j)\psi_n(j, z)}{k^2 - m_n^2(j)}, \quad (\text{XV.188})$$

which satisfies the boundary conditions $\partial_z h(j = 2, k, z_0) = 0$. We define a decay constant function (not exactly the decay constant) of the spin- j glueballs as

$$F_n(j) \equiv \frac{C(j, k, \epsilon)}{\sqrt{2}\kappa} (-\sqrt{g} e^{-\phi} |g^{xx}| \partial_{z'} \psi_n(j, z'))|_{z'=\epsilon}, \quad (\text{XV.189})$$

The normalized wave functions of the spin- j glueballs $\psi_n(j, z)$ satisfy the normalization condition

$$\int dz \sqrt{g} e^{-\phi} |g^{xx}| \psi_n(j, z) \psi_m(j, z) = \delta_{nm}. \quad (\text{XV.190})$$

For example, in the hard-wall model, the summation over n in (XV.188) can be carried out analytically and is given by

$$h(j, k, z) = -\sqrt{2}\kappa \sum_n \frac{F_n(j)\psi_n(j, z)}{k^2 - m_n^2(j)} = z^2 \left(\frac{A(j, k, z_0)}{B(j, k, z_0)} J_{\bar{\Delta}(j)}(kz) - Y_{\bar{\Delta}(j)}(kz) \right), \quad (\text{XV.191})$$

with

$$\begin{aligned} A(j, k, z_0) &= \partial_z (z^2 Y_{\bar{\Delta}(j)}(kz))|_{z=z_0}, \\ B(j, k, z_0) &= \partial_z (z^2 J_{\bar{\Delta}(j)}(kz))|_{z=z_0}, \end{aligned} \quad (\text{XV.192})$$

We also define

$$C(j, k, \epsilon) = h(j, k, \epsilon) \approx -\epsilon^2 Y_{\bar{\Delta}(j)}(k\epsilon). \quad (\text{XV.193})$$

For space-like momenta $k^2 = -K^2$: the non-normalizable wave function for the virtual transverse-traceless graviton is generally given by

$$\mathcal{H}(j, K, z) = \sqrt{2}\kappa \sum_n \frac{\mathcal{F}_n(j)\psi_n(j, z)}{K^2 + m_n^2(j)}, \quad (\text{XV.194})$$

which satisfies the IR boundary conditions $\partial_z \mathcal{H}(j = 2, K, z_0) = 0$. We have defined a decay constant function (for space-like momenta) of the spin- j glueballs as

$$\mathcal{F}_n(j) \equiv -\frac{\mathcal{C}(j, k, \epsilon)}{\sqrt{2}\kappa} (-\sqrt{g} e^{-\phi} |g^{xx}| \partial_{z'} \psi_n(j, z'))|_{z'=\epsilon}, \quad (\text{XV.195})$$

In the hard-wall model, the summation in (XV.194) reduces to

$$\mathcal{H}(j, K, z) = \sqrt{2}\kappa \sum_n \frac{\mathcal{F}_n(j)\psi_n(j, z)}{K^2 + m_n^2(j)} = z^2 \left(\frac{\mathcal{A}(j, K, z_0)}{\mathcal{B}(j, K, z_0)} I_{\bar{\Delta}(j)}(Kz) + K I_{\bar{\Delta}(j)}(Kz) \right), \quad (\text{XV.196})$$

with

$$\begin{aligned} \mathcal{A}(j, K, z_0) &= \partial_z (z^2 K I_{\bar{\Delta}(j)}(Kz))|_{z=z_0}, \\ \mathcal{B}(j, K, z_0) &= \partial_z (z^2 I_{\bar{\Delta}(j)}(Kz))|_{z=z_0}, \end{aligned} \quad (\text{XV.197})$$

We also define

$$\mathcal{C}(j, K, \epsilon) = \mathcal{H}(j, K, \epsilon) \approx \epsilon^2 K I_{\bar{\Delta}(j)}(K\epsilon). \quad (\text{XV.198})$$

For time-like momenta $k^2 > 0$: the bulk-to-bulk propagator for the massive spin- j glueballs, can be written as

$$\begin{aligned}\bar{G}_{\mu\nu\alpha\beta}^{TT}(j, z, z') &= \frac{1}{2} \left(\mathcal{T}_{\mu\alpha}(j)\mathcal{T}_{\nu\beta}(j) + \mathcal{T}_{\mu\beta}(j)\mathcal{T}_{\nu\alpha}(j) - \frac{2}{3}\mathcal{T}_{\mu\nu}(j)\mathcal{T}_{\alpha\beta}(j) \right) \bar{G}(j, z, z') \\ \bar{G}(j, z, z') &= z^{-(j-2)} G(j, z, z') z'^{-(j-2)} = \sum_n \frac{\tilde{\psi}_n(j, z)\tilde{\psi}_n(j, z')}{k^2 - m_n^2(j)},\end{aligned}\tag{XV.199}$$

and $\mathcal{T}_{\mu\nu}(j) = -\eta_{\mu\nu} + k_\mu k_\nu / m_n^2(j)$. For space-like momenta, we simply replace $k^2 = -K^2$ in (XV.199). Also remember that

$$h(j, k, z) = C(j, k, \epsilon) \sqrt{g} e^{-\phi} |g^{xx}| \partial_{z'} G(j, z, z')|_{z'=\epsilon}.\tag{XV.200}$$

Note that for $z \rightarrow 0$, we can approximately write the bulk-to-bulk propagator $G(j, z, z') = \sum_n \frac{\psi_n(z)\psi_n(z')}{k^2 - m_n^2(j)}$ in (XV.199) in terms of the unnormalized bulk-to-boundary propagator $h(j, k, z')$ as

$$G(j, z \rightarrow 0, z') \approx \frac{\psi_n(z \rightarrow 0)}{(-\sqrt{2\kappa})F_n(j)} \times (-\sqrt{2\kappa}) \sum_n \frac{F_n(j)\psi_n(z')}{k^2 - m_n^2(j)} = \frac{2^{-\tilde{\Delta}(j)} \times k^{\tilde{\Delta}(j)} \times z^{\tilde{\Delta}(j)+2}}{\tilde{\Delta}(j) + 2} h(j, k, z'),\tag{XV.201}$$

where we used

$$F_n(j) = \frac{C(j, k, \epsilon)}{\sqrt{2\kappa}} (-\sqrt{g} e^{-\phi} |g^{xx}| \partial_{z'} \psi_n(j, z'))|_{z'=\epsilon} = -\frac{1}{\sqrt{2\kappa}} \frac{2^{\tilde{\Delta}(j)}}{\pi} c_n(j) \left(\frac{m_n(j)}{k}\right)^{\tilde{\Delta}(j)} (2 + \tilde{\Delta}(j)) \frac{\Gamma(\tilde{\Delta}(j))}{\Gamma(1 + \tilde{\Delta}(j))},\tag{XV.202}$$

with $\psi_n(z \rightarrow 0) \approx \frac{2^{-\tilde{\Delta}(j)}}{\Gamma[1 + \tilde{\Delta}(j)]} c_n(j) (m_n)^{\tilde{\Delta}(j)} z^{\tilde{\Delta}(j)+2}$, and $C(j, k, \epsilon) = \frac{1}{k^2} (k\epsilon)^{2-\tilde{\Delta}(j)} \frac{2^{\tilde{\Delta}(j)}}{\pi} \Gamma(\tilde{\Delta}(j))$ for the hard-wall.

For space-like momenta $k^2 > 0$: we also have

$$G(j, z \rightarrow 0, z') \approx \frac{\psi_n(z \rightarrow 0)}{(\sqrt{2\kappa})\mathcal{F}_n(j)} \times (\sqrt{2\kappa}) \sum_n \frac{\mathcal{F}_n(j)\psi_n(z')}{K^2 + m_n^2(j)} = \frac{2^{1-\tilde{\Delta}(j)} \times K^{\tilde{\Delta}(j)} \times z^{\tilde{\Delta}(j)+2}}{\tilde{\Delta}(j) + 2} \mathcal{H}(j, K, z'),\tag{XV.203}$$

where we used

$$\mathcal{F}_n(j) = -\frac{\mathcal{C}(j, K, \epsilon)}{\sqrt{2\kappa}} (-\sqrt{g} e^{-\phi} |g^{xx}| \partial_{z'} \psi_n(j, z'))|_{z'=\epsilon} = \frac{1}{\sqrt{2\kappa}} 2^{\tilde{\Delta}(j)-1} c_n(j) \left(\frac{m_n(j)}{K}\right)^{\tilde{\Delta}(j)} (2 + \tilde{\Delta}(j)) \frac{\Gamma(\tilde{\Delta}(j))}{\Gamma(1 + \tilde{\Delta}(j))},\tag{XV.204}$$

with

$$\begin{aligned}\psi_n(z \rightarrow 0) &\approx \frac{2^{-\tilde{\Delta}(j)}}{\Gamma[1 + \tilde{\Delta}(j)]} c_n(j) (m_n)^{\tilde{\Delta}(j)} z^{\tilde{\Delta}(j)+2} \\ \mathcal{C}(j, K, \epsilon) &= \frac{1}{K^2} (K\epsilon)^{2-\tilde{\Delta}(j)} 2^{\tilde{\Delta}(j)-1} \Gamma(\tilde{\Delta}(j))\end{aligned}\tag{XV.205}$$

for the hard-wall model. Also remember that

$$\mathcal{H}(j, K, z) = -\mathcal{C}(j, K, \epsilon) \sqrt{g} e^{-\phi} |g^{xx}| \partial_{z'} G(j, z, z')|_{z'=\epsilon}. \quad (\text{XV.206})$$

2. Soft wall

The same relationships hold for the soft-wall model, where the spin- j glueballs' normalized wavefunctions are given in terms of the generalized Laguerre polynomials as [51] (note that the discussion in [51] is for general massive bulk scalar fluctuations but can be used for spin- j glueballs which have an effective bulk action (or bulk

equation of motion) similar to massive bulk scalar fluctuations [55])

$$\psi_n(j, z) = c_n(j) z^\Delta L_n^{\Delta(j)-2}(2\xi), \quad (\text{XV.207})$$

where $\xi = \tilde{\kappa}_N^2 z^2$, and the normalization coefficients are

$$c_n(j) = \left(\frac{2^{\Delta(j)} \tilde{\kappa}_N^{2(\Delta(j)-1)} \Gamma(n+1)}{\Gamma(n+\Delta(j)-1)} \right)^{\frac{1}{2}}. \quad (\text{XV.208})$$

The non-normalized bulk-to-boundary propagators for spin- j glueballs are given in terms of Kummer's (confluent hypergeometric) function of the second kind and its integral representation as (for space-like momenta $k^2 = -K^2$)

$$\begin{aligned} \mathcal{H}(j, K, z) &= z^\Delta U\left(a_K + \frac{\Delta(j)}{2}, \Delta(j) - 1; 2\xi\right) = z^{\Delta(j)} (2\xi)^{2-\Delta(j)} U\left(\tilde{a}(j), \tilde{b}(j); 2\xi\right) \\ &= z^{\Delta(j)} (2\xi)^{2-\Delta(j)} \frac{1}{\Gamma(\tilde{a}(j))} \int_0^1 dx x^{\tilde{a}(j)-1} (1-x)^{-\tilde{b}(j)} \exp\left(-\frac{x}{1-x} (2\xi)\right), \end{aligned} \quad (\text{XV.209})$$

where

$$\begin{aligned} a_K &= \frac{a}{2} = \frac{K^2}{8\tilde{\kappa}_N^2} \\ \tilde{a}(j) &= a_K + 2 - \frac{\Delta(j)}{2} \\ \tilde{b}(j) &= 3 - \Delta(j) \end{aligned} \quad (\text{XV.210})$$

and we have used the transformation $U(m, n; y) = y^{1-n} U(1+m-n, 2-n, y)$. The bulk-to-bulk propagator can also be approximated as (for space-like momenta $k^2 = -K^2$)

$$G(j, z \rightarrow 0, z') \approx \frac{\psi_n(z \rightarrow 0)}{(\sqrt{2\kappa}) \mathcal{F}_n(j)} \times (\sqrt{2\kappa}) \sum_n \frac{\mathcal{F}_n(j) \psi_n(z')}{K^2 + m_n^2(j)} = \frac{2^{\Delta(j)-2} \Gamma(a_K + \frac{\Delta(j)}{2})}{\Gamma(\Delta(j)-2)} \times \tilde{\kappa}_N^{2\Delta(j)-4} \times z^{\Delta(j)} \mathcal{H}(j, K, z'), \quad (\text{XV.211})$$

where we used

$$\begin{aligned} \mathcal{F}_n(j) &= -\frac{\mathcal{C}(j, K, \epsilon)}{\sqrt{2\kappa}} (-\sqrt{g} e^{-\phi} |g^{xx}| \partial_{z'} \psi_n(j, z'))|_{z'=\epsilon}, \\ \mathcal{C}(j, K, \epsilon) &= \mathcal{H}(j, K, \epsilon) \end{aligned} \quad (\text{XV.212})$$

and the substitution $\psi_n(z \rightarrow 0) \approx c_n(j) z^\Delta L_n^{\Delta(j)-2}(0)$ for the soft-wall model.

- [1] E. A. Kuraev, L. N. Lipatov and V. S. Fadin, Sov. Phys. JETP **45**, 199 (1977) [Zh. Eksp. Teor. Fiz. **72**, 377 (1977)].
 [2] I. I. Balitsky and L. N. Lipatov, Sov. J. Nucl. Phys. **28**,

- 822 (1978) [Yad. Fiz. **28**, 1597 (1978)].
 [3] J. M. Maldacena, Int. J. Theor. Phys. **38**, 1113 (1999) [Adv. Theor. Math. Phys. **2**, 231 (1998)] [hep-th/9711200]; S. S. Gubser, I. R. Klebanov and

- A. M. Polyakov, Phys. Lett. B **428**, 105 (1998) [hep-th/9802109]; E. Witten, Adv. Theor. Math. Phys. **2**, 505 (1998) [hep-th/9803131]; I. R. Klebanov and E. Witten, Nucl. Phys. B **556**, 89 (1999) [hep-th/9905104].
- [4] M. S. Costa, M. Djuric and N. Evans, JHEP **1309**, 084 (2013) [arXiv:1307.0009 [hep-ph]].
- [5] C. H. Lee, H. Y. Ryu and I. Zahed, Phys. Rev. D **98**, no. 5, 056006 (2018) [arXiv:1804.09300 [hep-ph]].
- [6] M. Rho, S. J. Sin and I. Zahed, Phys. Lett. B **466**, 199 (1999) [hep-th/9907126].
- [7] R. A. Janik and R. B. Peschanski, Nucl. Phys. B **586**, 163 (2000) [hep-th/0003059].
- [8] R. C. Brower, J. Polchinski, M. J. Strassler and C. I. Tan, JHEP **0712**, 005 (2007) [hep-th/0603115]; R. C. Brower, M. J. Strassler and C. I. Tan, JHEP **0903**, 092 (2009) [arXiv:0710.4378 [hep-th]]; R. C. Brower, M. S. Costa, M. Djuric, T. Raben and C. I. Tan, JHEP **1502**, 104 (2015) [arXiv:1409.2730 [hep-th]].
- [9] A. Stoffers and I. Zahed, Phys. Rev. D **87**, 075023 (2013) [arXiv:1205.3223 [hep-ph]]; A. Stoffers and I. Zahed, Phys. Rev. D **88**, no. 2, 025038 (2013) [arXiv:1211.3077 [nucl-th]].
- [10] A. Stoffers and I. Zahed, arXiv:1210.3724 [nucl-th].
- [11] G. Basar, D. E. Kharzeev, H. U. Yee and I. Zahed, Phys. Rev. D **85**, 105005 (2012) [arXiv:1202.0831 [hep-th]].
- [12] Y. Hatta, E. Iancu and A. H. Mueller, JHEP **0801**, 026 (2008) [arXiv:0710.2148 [hep-th]].
- [13] Y. Hatta, T. Ueda and B. W. Xiao, JHEP **0908**, 007 (2009) [arXiv:0905.2493 [hep-ph]].
- [14] J. Nemchik, N. N. Nikolaev and B. G. Zakharov, Phys. Lett. B **341**, 228 (1994) [hep-ph/9405355]; J. Nemchik, N. N. Nikolaev, E. Predazzi and B. G. Zakharov, Phys. Lett. B **374**, 199 (1996) [hep-ph/9604419]; J. Nemchik, N. N. Nikolaev, E. Predazzi and B. G. Zakharov, Z. Phys. C **75**, 71 (1997) [hep-ph/9605231]; H. G. Dosch, T. Goussset, G. Kulzinger and H. J. Pirner, Phys. Rev. D **55**, 2602 (1997) [hep-ph/9608203]; G. Kulzinger, H. G. Dosch and H. J. Pirner, Eur. Phys. J. C **7**, 73 (1999) [hep-ph/9806352]; H. G. Dosch and E. Ferreira, Eur. Phys. J. C **51**, 83 (2007) [hep-ph/0610311, arXiv:0905.0193 [hep-ph]]; G. Chen, Y. Li, P. Maris, K. Tuchin and J. P. Vary, Phys. Lett. B **769**, 477 (2017) [arXiv:1610.04945 [nucl-th]]; N. Nikolaev and B. G. Zakharov, Z. Phys. C **53**, 331 (1992); A. H. Mueller and B. Patel, Nucl. Phys. B **425**, 471 (1994) [hep-ph/9403256]; J. R. Forshaw, G. Kerley and G. Shaw, Phys. Rev. D **60**, 074012 (1999) [hep-ph/9903341]; J. R. Forshaw, G. R. Kerley and G. Shaw, Nucl. Phys. A **675**, 80C (2000) [hep-ph/9910251]; M. McDermott, R. Sandapen and G. Shaw, Eur. Phys. J. C **22**, 655 (2002) [hep-ph/0107224]; K. J. Golec-Biernat and M. Wusthoff, Phys. Rev. D **59**, 014017 (1998) [hep-ph/9807513]; K. J. Golec-Biernat and M. Wusthoff, Phys. Rev. D **60**, 114023 (1999) [hep-ph/9903358]; E. Iancu, K. Itakura and S. Munier, Phys. Lett. B **590**, 199 (2004) [hep-ph/0310338]; J. R. Forshaw, R. Sandapen and G. Shaw, Phys. Rev. D **69**, 094013 (2004) [hep-ph/0312172]; C. Marquet, R. B. Peschanski and G. Soyez, Phys. Rev. D **76**, 034011 (2007) [hep-ph/0702171 [HEP-PH]]; J. R. Forshaw and R. Sandapen, JHEP **1110**, 093 (2011) [arXiv:1104.4753 [hep-ph]].
- [15] A. Ali *et al.* [GlueX Collaboration], Phys. Rev. Lett. **123**, no. 7, 072001 (2019) [arXiv:1905.10811 [nucl-ex]].
- [16] K. Hafidi, S. Joosten, Z. E. Meziani and J. W. Qiu, Few Body Syst. **58** (2017) no.4, 141; S. Joosten and Z. E. Meziani, PoS QCDEV **2017**, 017 (2018) [arXiv:1802.02616 [hep-ex]].
- [17] Y. Hatta and D. L. Yang, Phys. Rev. D **98**, no. 7, 074003 (2018) [arXiv:1808.02163 [hep-ph]].
- [18] Y. Hatta, A. Rajan and D. L. Yang, Phys. Rev. D **100**, no. 1, 014032 (2019) [arXiv:1906.00894 [hep-ph]].
- [19] D. Kharzeev, H. Satz, A. Syamtomov and G. Zinovjev, Eur. Phys. J. C **9**, 459 (1999) [hep-ph/9901375]; S. J. Brodsky, E. Chudakov, P. Hoyer and J. M. Laget, Phys. Lett. B **498**, 23 (2001) [hep-ph/0010343].
- [20] M. Srednicki, "Quantum field theory," Ed. J. Wiley 2010.
- [21] Z. Abidin and C. E. Carlson, Phys. Rev. D **79**, 115003 (2009) [arXiv:0903.4818 [hep-ph]].
- [22] E. D'Hoker and B. Pourhamzeh, JHEP **1606**, 146 (2016) [arXiv:1602.01487 [hep-th]].
- [23] I. Kirsch, JHEP **0609**, 052 (2006) [hep-th/0607205].
- [24] H. R. Grigoryan, P. M. Hohler and M. A. Stephanov, Phys. Rev. D **82**, 026005 (2010) [arXiv:1003.1138 [hep-ph]].
- [25] I. Kanitscheider, K. Skenderis and M. Taylor, JHEP **0809**, 094 (2008) [arXiv:0807.3324 [hep-th]].
- [26] P. E. Shanahan and W. Detmold, Phys. Rev. D **99** (2019) no.1, 014511 [arXiv:1810.04626 [hep-lat]].
- [27] M. V. Polyakov and P. Schweitzer, Int. J. Mod. Phys. A **33**, no. 26, 1830025 (2018) [arXiv:1805.06596 [hep-ph]].
- [28] P. E. Shanahan and W. Detmold, Phys. Rev. Lett. **122**, no. 7, 072003 (2019) [arXiv:1810.07589 [nucl-th]].
- [29] V. D. Burkert, L. Elouadrhiri and F. X. Girod, Nature **557**, no. 7705, 396 (2018).
- [30] U. Camerini *et al.*, Phys. Rev. Lett. **35**, 483 (1975).
- [31] B. Gittelman, K. M. Hanson, D. Larson, E. Loh, A. Silverman and G. Theodosiou, Phys. Rev. Lett. **35**, 1616 (1975).
- [32] R. Barate *et al.* [NA14 Collaboration], Z. Phys. C **33** (1987) 505.
- [33] C. Adloff *et al.* [H1 Collaboration], Eur. Phys. J. C **13**, 371 (2000) [hep-ex/9902019].
- [34] M. E. Binkley *et al.*, Phys. Rev. Lett. **48**, 73 (1982).
- [35] S. Chekanov *et al.* [ZEUS Collaboration], Eur. Phys. J. C **24**, 345 (2002) [hep-ex/0201043].
- [36] A. Aktas *et al.* [H1 Collaboration], Eur. Phys. J. C **46**, 585 (2006) [hep-ex/0510016].
- [37] C. Alexa *et al.* [H1 Collaboration], Eur. Phys. J. C **73**, no. 6, 2466 (2013) [arXiv:1304.5162 [hep-ex]].
- [38] R. Aaij *et al.* [LHCb Collaboration], J. Phys. G **40**, 045001 (2013) [arXiv:1301.7084 [hep-ex]].
- [39] J. Breitweg *et al.* [ZEUS Collaboration], Phys. Lett. B **437**, 432 (1998) [hep-ex/9807020].
- [40] C. Adloff *et al.* [H1 Collaboration], Phys. Lett. B **483**, 23 (2000) [hep-ex/0003020].
- [41] S. Chekanov *et al.* [ZEUS Collaboration], Phys. Lett. B **680**, 4 (2009) [arXiv:0903.4205 [hep-ex]].
- [42] R. Aaij *et al.* [LHCb Collaboration], JHEP **1509**, 084 (2015) [arXiv:1505.08139 [hep-ex]].
- [43] A. M. Sirunyan *et al.* [CMS Collaboration], Eur. Phys. J. C **79**, no. 3, 277 (2019) [arXiv:1809.11080 [hep-ex]].
- [44] A. V. Belitsky and A. V. Radyushkin, Phys. Rept. **418**, 1 (2005) [hep-ph/0504030].
- [45] A. Vega, I. Schmidt, T. Gutsche and V. E. Lyubovitskij, Phys. Rev. D **83**, 036001 (2011) [arXiv:1010.2815 [hep-ph]].
- [46] X. D. Ji, Phys. Rev. Lett. **78**, 610 (1997) [hep-ph/9603249].

- [47] H. R. Grigoryan and A. V. Radyushkin, Phys. Lett. B **650**, 421 (2007) [hep-ph/0703069].
- [48] Z. Abidin and C. E. Carlson, Phys. Rev. D **77**, 095007 (2008) [arXiv:0801.3839 [hep-ph]].
- [49] H. R. Grigoryan and A. V. Radyushkin, Phys. Rev. D **76**, 095007 (2007) [arXiv:0706.1543 [hep-ph]].
- [50] S. Hong, S. Yoon and M. J. Strassler, JHEP **0604**, 003 (2006) [hep-th/0409118].
- [51] C. A. Ballon Bayona, H. Boschi-Filho and N. R. F. Braga, JHEP **0803**, 064 (2008) [arXiv:0711.0221 [hep-th]].
- [52] J. H. Gao and B. W. Xiao, Phys. Rev. D **81**, 035008 (2010) [arXiv:0912.4333 [hep-ph]].
- [53] S. Raju, Phys. Rev. D **83**, 126002 (2011) [arXiv:1102.4724 [hep-th]].
- [54] E. D'Hoker, D. Z. Freedman, S. D. Mathur, A. Matusis and L. Rastelli, Nucl. Phys. B **562**, 330 (1999) [hep-th/9902042].
- [55] J. Polchinski and M. J. Strassler, Phys. Rev. Lett. **88**, 031601 (2002) [hep-th/0109174]; R. C. Brower, M. J. Strassler and C. I. Tan, JHEP **0903**, 092 (2009) [arXiv:0710.4378 [hep-th]].